Journal of Fusion Energy, Vol. 9, No. 1, 1990

An FEL-Based Microwave System for Fusion

R. R. Stone,[1] R. A. Jong,[1] T. J. Orzechowski,[1] E. T. Scharlemann,[1] A. L. Throop,[1] B. Kulke,[1] K. I. Thomassen,[1] and B. W. Stallard[1]

This paper describes designs for 280-GHz and 560-GHz microwave sources based on free electron lasers (FELs). These 10-MW units are based on technology developed over the last 5 years. A first demonstration of high-average-power microwave production with an FEL system is expected in the Microwave Tokamak Experiment (MTX) facility. This paper gives details on the design and construction of that 250-GHz, 2-MW system and discusses specific applications for the Compact Ignition Tokamak (CIT).

KEY WORDS: Compact Ignition Tokamak (CIT); Experimental Test Accelerator-II (ETA-II); free electron laser (FEL); Intense Mircowave Prototype (IMP); International Thermonuclear Experimental Reactor (ITER); microwave generation; Microwave Tokamak Experiment (MTX); wiggler.

1. INTRODUCTION

In the past 5 years, the single-pulse demonstration of microwave generation with induction linac free electron lasers (IFEL) has led to strong interest in the application of this technology for fusion. Paralleling this work, the development and testing of high-repetition-rate pulsed power chains to drive these induction accelerators has made high average power FEL microwave generation a possibility.

The interest in this technology stems from the ease of generation of high-frequency microwaves, the board bandwidth of the amplifier, the tunability of the center frequency, and the high average power per unit with the new magnetic switching technology. A demonstration of these principles is expected over the next several years in the Microwave Tokamak Experiment (MTX) at Lawrence Livermore National Laboratory (LLNL).[1] For that application, a 2-MW average power source at 250 GHz is being constructed. The 8-GW, 50-ns pulses are to be repeated every 200 μs to produce this power.

[1] Lawrence Livermore National Laboratory, Livermore, California, 94550.

This paper describes a 10-MW system for the Compact Ignition Tokamak (CIT), based on the technologies used in the MTX design. It differs primarily in having a 10-kHz repetition rate instead of 5 kHz, a 70-ns pulse rather than 50 ns, and a 13-MeV electron beam rather than 10 MeV. The power and energy per pulse are 14 GW and 1 kJ for CIT, compared with 8 GW and 400 J in MTX.

1.1. Physics Issues

The absorption mechanisms for intense pulses from the IFEL are nonlinear, and this new regime required detailed studies to determine the wave interaction physics. Nonlinear mechanisms also can influence the propagation of these pulses to the resonance zones. Propagation, as described by conventional ray processes, may be altered by three-wave (and four-wave) parametric processes, by ponderomotive forces, or by scattering from plasma fluctuations. Each of these physics issues has been theoretically addressed, and a discussion of results for CIT applications follows.

Absorption is modified[2] from that given by linear

0164-0313/90/0300-0077$06.00/0

theory in that both the opacity and absorption are changed. The linear absorption theory predicts an optical thickness τ (transmitted power diminishes exponentially in τ),

$$\tau = \pi^2(R/\lambda)(T/mc^2)f(\alpha)$$

with major radius R, wavelength λ, temperature T in keV (with $mc^2 = 511$ keV), and α the ratio ω_p^2/ω^2. For first harmonic ordinary mode (280 GHz) near perpendicular incidence,

$$f(\alpha) = \alpha(1 - \alpha)^{1/2}$$

so that at 280 GHz, 10-T operation, with $\alpha = 3/4$ (near density for maximum abosorption), the optical thickness is ≈ 30 in CIT (using $R = 2.2$ m, $T = 2$ keV in early ohmic phase). The wave is cut off for densities $n_{14} \geq 9.7$, or $\alpha = 1$. For $\alpha << 1$, we find $\tau \approx 80\alpha$.

Nevins[3] has given an estimate for the nonlinear optical thickness, which underestimates absorption since it neglects changes in parallel wave number along the electron orbit through the wave. Thus, the important physics of "bucket lifting" is left out of this estimate, an omission which results in a lower value of τ_{nl} than the correct one. His formula is

$$\tau_{nl} \approx 32 n_{14} T^{7/6}_{\text{keV}} (1-\alpha)^{2/3} h^{1/3} W^{-1/3}_{\text{fel}} B_T^{-4/3} w^{-2/3}$$

Here, the wave packet has a height h (cm) and width w (cm), and the energy in the pulse is W_{fel}. For $n_{14} = (3/4) \times 9.7$, $T = 2$ keV, $\alpha = 3/4$, $h = 30$ cm, $w = 20$ cm, $B = 10$ T, $W_{\text{fel}} = 1000$, we get $\tau_{nl} = 1.28$. Thus, essentially all the power is absorbed even at 2 keV. A better estimate can be made using a Monte Carlo code developed by Rognlien.[4] This code includes changes both in the magnetic field and the parallel wave number along the orbit, both of which change the Doppler-shifted resonance condition. Aiming of the wave off-centerline introduces more field variation since the poloidal field varies with radius, and causing the beam to diverge from the final focusing mirror will vary the parallel wave number. These are both important effects, and combined, they can significantly raise the absorption coefficient to values approaching the linear one. In earlier studies of the CIT application, Rognlien[5] found that these effects lead to an order-of-magnitude increase in the optical thickness in CIT for realistic parameters.

Nonlinear, whole-beam self-focusing can occur when the wave electric field intensity E is large. The ponderomotive force, proportional to the gradient of E^2, gives rise to quasi-steady plasma response,

$$n = n_o \exp[-e^2E^2/2m\omega^2(T_e + T_i)]$$

This local depression in density leads to a local increase in the plasma dielectric constant in the wave path, thus bending the rays so as to focus the wave. It was first shown by Cardinali *et al.*[6] and later by Cohen[7] that in MTX this results in filamentation of the wave at a distance of 25–30 cm into the plasma, fortunately beyond the resonance layer. The focus forms in a time less than the FEL pulse length, and the focal distance is initially far away but rapidly approaches a distance ℓ consistent with the steady-state relationship given by Max,[8]

$$\ell/\lambda = 2\pi^2(a_e/\lambda)^2(8y)^{-1/2}$$

with λ the wavelength in the plasma and

$$\pi a_e \sqrt{2y} = (c/f_{pe})\exp(y/2)$$

The quantity y is defined by

$$4[(1 + T_i/T_e)]y = (v_o/v_{th})^2$$

Here, v_o is the electron oscillation velocity in the wave electric field, v_{th} the electron thermal velocity T_e/m_e; and f_{pe} the electron plasma frequency. For CIT, with its larger wave area, the electric field (about 100 kV/cm) is one-fifth as large as in MTX, even though the power in each pulse is nearly doubled. Also, temperatures in CIT are much higher (by a factor of 5), which considerably alleviates the ponderomotive effects. Indeed, the above formulation shows a focal point at $\ell \approx 55$ m.

Of the various three-wave processes studied in detail by Porkolab and Cohen,[9] only one was found to be of concern. Others are potentially important, but they are absorptive. In MTX, background fluctuations at the ion cyclotron frequency are amplified (to a level limited by convection out of the region where the instability threshold is exceeded), and these fluctuations backscatter a portion of the incident wave. The initial level of the fluctuations must be 3–4 orders of magnitude above thermal before a significant fraction of the incident wave is reflected. In CIT, with lower electric field strength, there is less concern over backscatter since the threshold depends on the square of the ratio of the oscillation velocity of electrons in the wave to their thermal velocity. The factor of 25 in E^2 and the increase in electron temperature by a factor of 5 reduce this ratio by 125 over that in MTX.

Finally, ECH waves can be scattered by turbulence at the edge of the plasma. The effective scattering distance ℓ_s depends on the square of the percent density fluctuations.[10,11] In CIT, as in MTX, even assuming 5% fluctuation levels, the scattering angle $\Delta\theta^2 \sim \Delta r/\ell_s$ is small. Here, Δr is the width of the turbulent region. These fluctuations, if present, would help counteract a tendency toward filamentation and would reduce growth rates of any parametric process.

1.2. Physics and Technology Base

1.2.1. Past Experience

The possibility of operating and modeling high peak power microwave FELs was sucessfully demonstrated at the Electron Laser Facility (ELF), the first LLNL microwave FEL experiment. The ELF experiments, now completed, were conducted at 35 and 140 GHz, with more than 1 GW of peak power at 35 GHz obtained from a tapered wiggler amplifier. At 140 GHz, the available input power and wiggler length limited operation to the exponential gain regime, but in both cases there was excellent agreement between numerical simulations and experimental data.

Further validation of the FEL simulation codes has been achieved at PALADIN, a 10.6-μm FEL experiment driven by the 50-MeV Advanced Test Accelerator (ATA). In a 15-m wiggler, a 43-MeV, 800-A electron beam produced 27 dB of exponential gain, again with good agreement between experiment and simulation.

Prototypes for most of the important components of a high-average-power microwave FEL have been constructed, with continuing acitivity in design and testing. Notable among these prototypes are the high-repetition-rate magnetic switching system units which have been operated at a 5-kHz repetition rate into a dummy load.

One-period prototypes of several high-field-strength wiggler designs have been built with various combinations of electromagnets and permanent magnets, and have been used to benchmark the LLNL wiggler design codes. The design of a 5.5-m wiggler to be used in the IMP/MTX experiment (described in Section 1.2.2) is nearly complete, with a single-period prototype built and tested. The wiggler will be completed in late 1989. For future fusion applications, higher field strengths can be obtained through the use of materials other than normal iron for the wiggler poles and yoke; the properties of these materials are now being explored.

1.2.2. Future Plans

An FEL referred to as the Intense Microwave Prototype (IMP) is being constructed for MTX to provide 250-GHz, 50-ns pulses, with up to 8 GW of peak power and 2 MW of average power. This FEL will use the Experimental Test Accelerator-II (ETA-II) to obtain a 10-MeV, 3-kA beam operating at 5 kHz for 0.5 s. The FEL will operate at both 140 and 250 GHz using a 5.5-m wiggler that will reach the required 4.5-kG field. With this system, critical plasma and FEL physics issues will be explored between FY89 and 91.

Code improvements are continuing for more accurately modeling microwaves in a wave guide. These codes will be validated against past results, the present LLNL codes, and future experiments.

A tuneable master oscillator for operation at 140 GHz is being developed. A prototype of the oscillator is currently being tested. The prototype will be scaleable to 10-kW output at 280 GHz and will tunable to ±3% within milliseconds.

Studies are underway to determine the feasibility of fabricating long (4–5 m) corrugated wave guides for use at 280 and 560 GHz. Short samples will be fabricated by electroforming, and an attempt will be made to join them, either by brazing or electron beam welding. Corrugated guides force the propagation of the HE_{11} mode and greatly reduce the radio frequency (rf) wall heating in the wiggler interaction region.

1.3. Baseline IFEL for Fusion Applications

Figure 1 shows the baseline configuration for an FEL to produce 10 MW average power at 280 GHz. The accelerator produces a 13-MeV, 3-kA beam with a brightness of 10^8 A/(rad-m)^2 and a flattop pulse width of 70 ns. The accelerator and power conditioning chain run at a maximum of 10 kHz. The beam transport line consists of the normal quadrupoles and dipoles with beam-steering coils to make minor adjustments in beam position at specific locations. The master oscillator is a tuneable backward wave oscillator (BWO) providing 500 W of fast tuneable power at the wiggler entrance. The 3-m-long wiggler has a 4-cm gap and a 10-cm period with a maximum magnetic field of 5.7 kG. Vanadium Per-

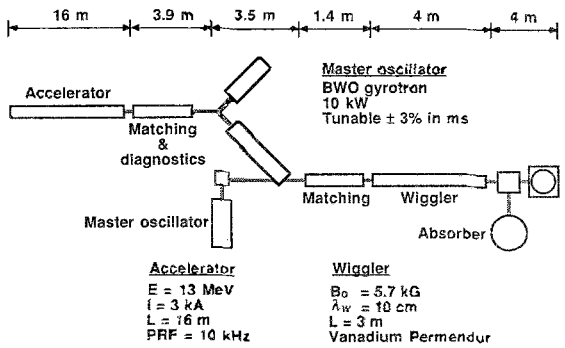

Fig. 1. Schematic of 280-GHz, 10-MW FEL with a PRF of 10 kHz for the accelerator and pulsed power chain. The major parameters for the master oscillator, accelerator, and the wiggler are shown.

mendur is used as the yoke and pole material to obtain the high field. The electron beam is turned out of the microwave line-of-sight by an Enge magnet, and the microwaves continue to the tokamak down a 50-cm-diam quasioptical transport system. The mirrors in this transport system are sized to reduce the losses and to preclude overheating of the copper surfaces. Pumping is provided throughout this transport line to reduce the amount of tritium diffusing from the fusion machine to the FEL. The electron beam is absorbed by using either a thermal inertial mass that is cooled between shots or high-velocity water that not only absorbs the electron beam energy but keeps a thin (2-mm) aluminum vacuum barrier cool. This configuration is expected to produce 70-ns pulses with a peak power of 14 GW and thus an average power of 10 MW at 10-kHz pulse repetition frequency (PRF). The configuration for 560-GHz operation requires an increased beam energy of 15 MeV, a slightly longer wiggler, and a different master oscillator.

If the schedules for MTX and other programs at LLNL are maintained, all the major physics and technology issues will be resolved prior to the requirement for a major commitment of resources in FY91.

2. PHYSICS AND TECHNOLOGY BASE

2.1. Past Experiments at 35 and 140 GHz

An FEL operating in the microwave (35 and 140 GHz) regime was constructed to study the basic physics of free electron lasers and to serve as a test bed for the physical models used in designing other FEL amplifiers. This experiment, the Electron Laser Facility (ELF), started operation in 1982. ELF was designed to use the electron beam from ETA, which was capable of producing 10 kA at 4.5 MeV. During the ELF experiments, a beam with about 1 kA of current of 3.5 MeV was typically used. By using the proper wiggler parameters, over 1 GW of peak power at 35 GHz was produced.[12–15]

Figure 2 shows a schematic of the facility, which consisted of an accelerator (ETA), an electron beam transport line with an emittance selector, a microwave source, and a wiggler. ELF was a single-pass FEL amplifier, which used a conventional microwave source as a master oscillator. This signal was injected into the wiggler line-of-sight by reflection off a wire mesh and propagated colinearly with the electron beam. Experiments were performed to observe the interaction of the microwaves and the electron beam by changing the wiggler length and magnetic field.

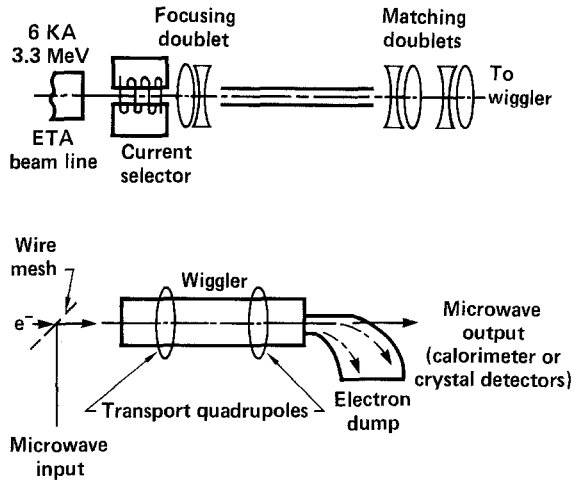

Fig. 2. Schematic of the Electron Laser Facility (ELF).

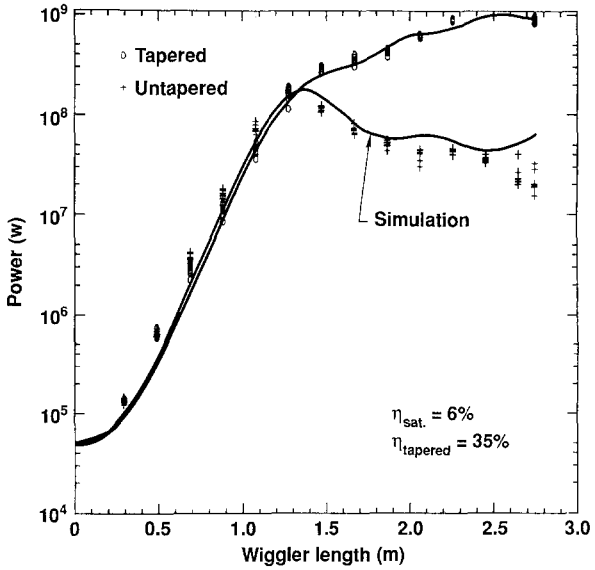

Fig. 3. Peak power of 35 GHz vs. wiggler length for a tapered and an untapered wiggler. Both experimental and simulation results are shown.

Figure 3 shows the results obtained at 35 GHz for a tapered and an untapered wiggler. Also shown are the results of numerical simulation.[16] About 1 GW of peak power in the TE_{01} mode was obtained by tapering the wiggler field. Other experiments indicated that, using the same wiggler magnetic field profile, the frequency could be changed plus or minus about 12% with a drop in peak power of only 1 dB.

Experiments were conducted at 140 GHz, and a

gain of about 20 dB/m in the exponential gain regime was obtained with a peak power of about 100 MW. The wiggler available was not long enough to allow operation above this regime. The numerical simulations at 140 GHz agreed well with the experimental results. These results confirmed our ability to produce high peak microwave power and to predict the FEL performance.

2.2. FEL Source for MTX

The technologies incorporated into the FEL for MTX are described here in some detail since they serve as the basis for the CIT system. In most cases, very little extrapolation is required to achieve the design performance for the 10-MW system for CIT.

2.2.1. Goals

MTX will be used as a development and demonstration testbed for electron cyclotron heating (ECH) of tokamak plasmas using intense microwave pulses from an IFEL. MTX will use the Alcator-C tokamak, which has been refurbished and relocated to LLNL from the Massachusetts Institute of Technology (MIT) Plasma Fusion Center. It is capable of operating at toroidal fields above 9 T so that the heating at high plasma densities using high-frequency sources that are of interest to CIT and the International Thermonuclear Experimental Reactor (ITER) can be investigated. The specific objectives of MTX are to study the technology, physics, and applications of ECH for tokamaks using the short-pulse heating provided by the IFEL.

These studies will require an FEL that can deliver 1–2 MW of average power at 250 GHz during the 0.5-s duration of the MTX shot. LLNL is constructing such a source using the ETA-II accelerator and a prototype of the high-field laced wiggler that will be described in a later section. This Intense Microwave Prototype (IMP) FEL is designed to produce up to 2 MW of average power at 250 GHz, with a peak power of 8 GW and a pulse width of 50 ns, and to operate at a 5-kHz PRF. This performance level will be achieved in several phases as the capability of ETA-II is increased.

The following sections describe the design and expected performance of the IMP FEL, the engineering issues being addressed, and the present status and plans.

2.2.2. Expected Performance

The design and capability of the IMP FEL are constrained by the expected performance of ETA-II and the high-field prototype wiggler, as shown in Fig. 4. Fortunately, the parameters of these systems are compatible with those required by MTX. Simulation codes were used to optimize the performance of the IMP FEL under these design constraints.

Simulation results of the IMP FEL are shown in Fig. 5, where axial profiles of the wiggler field and the corresponding FEL peak power are plotted. Due to space charge effects, a "Raman" taper is used in the wiggler field profile.[17] Over the constant-field gain region of the wiggler, the field is held so that the signal is amplified at the peak of the gain curve, and slightly below the field for FEL synchronism, to achieve good exponential gain and trapping efficiency. Prior to saturation of FEL growth, the wiggler field is changed to achieve synchronism between the electron beam bunches and the ponderomotive well. This minimizes detrapping in the tapered region and optimizes overall conversion efficiency.

As shown in Fig. 5, simulations predict an exponential gain of 31 dB/m, power at saturation of more than 1 GW, and a peak output power of about 12 GW for an optimized taper if system errors are not considered. System errors, discussed later, are expected to reduce the peak output power to about 11 GW. This reduced level corresponds to a peak conversion efficiency of 39% and a total amplifier gain of 73 dB. For this design, the limitation on output power has been determined by the minimum wiggler field that will keep the linear beam fill factor at less than 50%. Although this is a somewhat

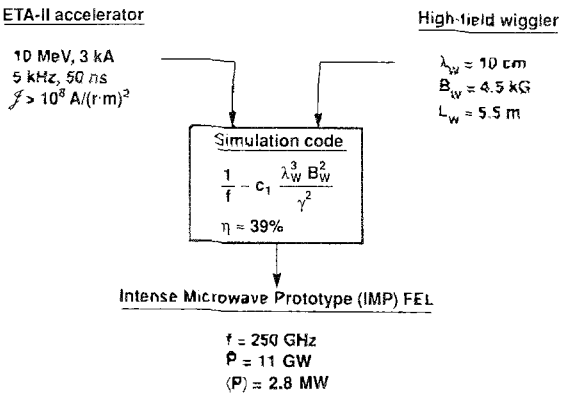

Fig. 4. Accelerator and wiggler parameters and used in design simulations for the IMP FEL for MTX.

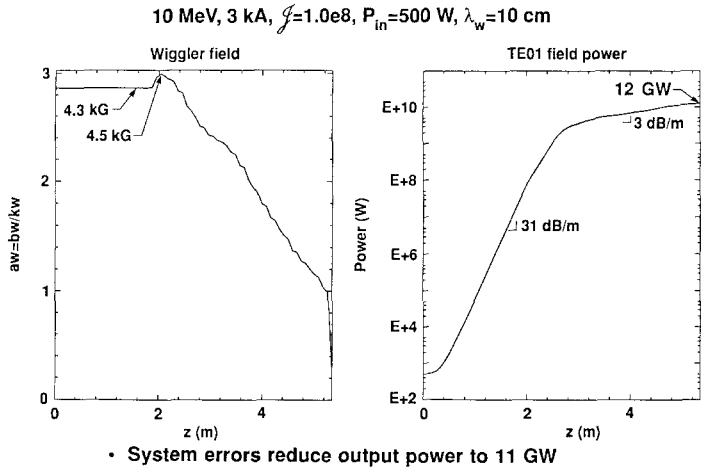

Fig. 5. Simulation results showing wiggler field and gain profiles at 250 GHz for IMP.

conservative value, it represents a practical tradeoff between performance and beam loss or transport issues in the wave guide.

As shown in Fig. 6, simulations predict good mode quality for strongly tapered FELs such as IMP. In the tapered region, the output power is predominantly in the resonant design mode (TE_{01} in the simulations). Microwave transport simulations show that the next-lowest mode (TE_{21}) is still transported with good efficiency from the FEL to the tokamak, although only a fraction (about 25%) is of the proper polarization to heat the plasma.

As described earlier, the ability to control the frequency of a high-power ECH source on a fast timescale (milliseconds) can be exploited for disruption control, heating during the plasma buildup, and other tokamak applications. Figure 7 shows the amplifier bandwidth expected for IMP, which is typical of IFEL performance at millimeter wavelengths. For these simulations, all beam and wiggler parameters were held constant, and only the frequency of the input signal was varied. The 3-dB fre-

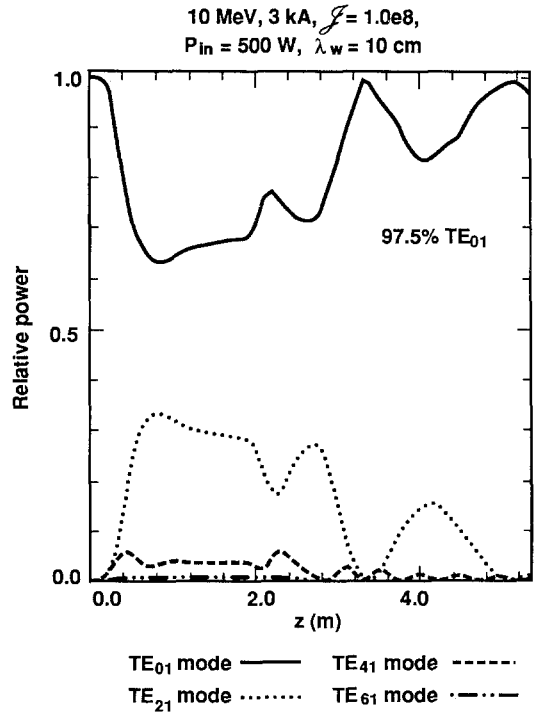

Fig. 6. Simulations of mode content for 250 GHz for IMP.

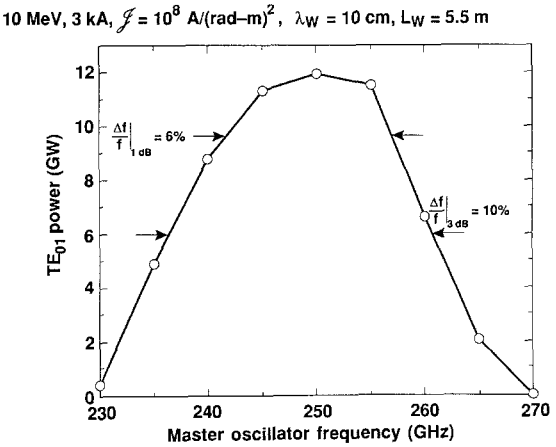

Fig. 7. Simulation results for 250 GHz showing the inherent bandwidth of the FEL.

quency bandwidth is 10% and represents the range over which the frequency of the high-power FEL output could be electronically tuned by controlling the frequency of the low-power master oscillator. If the wiggler taper is further optimized, a broader frequency range of about 15–20% can be achieved on a timescale of minutes. With further changes in beam energy, the operational range can be further extended.

A parametric study was made for the above baseline case, examining the sensitivity of IMP performance on system errors and noise. The results are summarized in Table I. A peak output power of 11 GW is predicted for combined-error limits of 0.1% RMS (root-mean-square) wiggler error, 1-mm offset of the beam in both the wiggle and nonwiggle planes, and ±1% beam energy sweep. These values represent errors that are achievable in the near future, and may be conservative in the light of the present FEL program-development goals.

The high extraction and trapping efficiency indicate that space charge effects have been largely compensated for by operating at higher beam energy and by using the Raman taper. The output noise power is 30 dB below the signal power, assuming an input power density of 13 dB over shot noise, and is roughly proportional to the input noise level. Even with system errors, there is design margin over the maximum IMP objective of 2-MW average power. Operation with a beam energy as low as 9 MeV can still achieve the design objective.

2.2.3. *Description of Major Subsystems*

The next five subsections describe the major subsystems that comprise the IMP FEL and address the engineering issues and the present status of each subsystem. In addition to ETA-II, these subsystems include the electron-beam transport system, the rf coupling and beam-matching beamline section, the wiggler system, and the microwave system.

Table I. Predicted Performance of the IMP FEL at 250 GHz[a]

Peak TE_{01} output power	12 GW (11 GW)
Average TE_{01} output power	2.8 GW
TE_{01} mode fraction	97%
Extraction efficiency	44% (39%)
Trapping efficiency	70%
Peak noise power	10 MW
3-dB amplifier bandwidth	10%
r_{beam}/r_{wall}	0.5

[a] Performance with errors in parentheses.

An overview of the 250-GHz FEL beamline and wiggler system is shown in Fig. 8. Figure 9 shows an elevation view of the wiggler and the microwave system, including the gyrotron master oscillator, rf coupler, and microwave transmission system from the FEL to MTX.

ETA-II Accelerator. To serve as a high-quality, high-power source of relativistic electrons for the IMP FEL, ETA-II must operate with the parameters shown in Table II. The performance requirements for IMP are within the design parameters of ETA-II and are significantly relaxed for two of the most critical parameters: beam brightness and energy regulation. To achieve operation at 9–10 MeV, two additional accelerator block sections will probably be needed, but this represents low technical risk. Achievement of the 3-kA beam current is aided by the greatly relaxed requirement on beam brightness. Off-line testing has demonstrated 5-kHz operation of major components in the pulsed-power chain for short bursts. While ETA-II represents a developmental program in its own right, achievement of high average power (HAP) operation is expected to occur by 1990 as the PRF and burst duration are increased to achieve the full 10 MW of average beam power.

The initial performance of ETA-II is shown in Table III. Due to poisoning by Freon, the cathode was emission-limited for this initial data set. This problem has since been corrected. The eventual goals for ETA-II are shown on Table IV.

Electron Beam Transport System. The electron beam transport system (Fig. 8) is used to transport, diagnose, and condition the HAP electron beam prior to injecting it into the wiggler. The transport system uses a series of solenoid and quadrupole magnets to transport the beam from the exit of the accelerator to the wiggler entrance. Beam ripple is minimized to avoid emittance growth. Diagnostics are provided in the beamline to measure beam current, energy, position, spatial shape, and brightness.

Handling the HAP electron beam is a critical design issue, since about 5 MJ of energy is contained in a 0.5-s shot. Fortunately, 0.5-s is sufficiently short for most designs so that thermal inertia can be used instead of active cooling. In the beamline, a small linear fill factor (<50%) for the electron beam is maintained to ensure minimal beam loss. An emittance filter consisting of a series of range-thin graphite apertures in the beamline is used to scatter any low-density halo electrons to the wall over a distributed area. At 5-kHz operation, a trigger-interrupt system is designed for ETA-II that will sense a significant loss of current during a 50-ns pulse and reduce the PRF to 1 Hz before subsequent pulses can damage any beamline components. During 10.6-μm FEL experiments at LLNL, beam current was transmitted

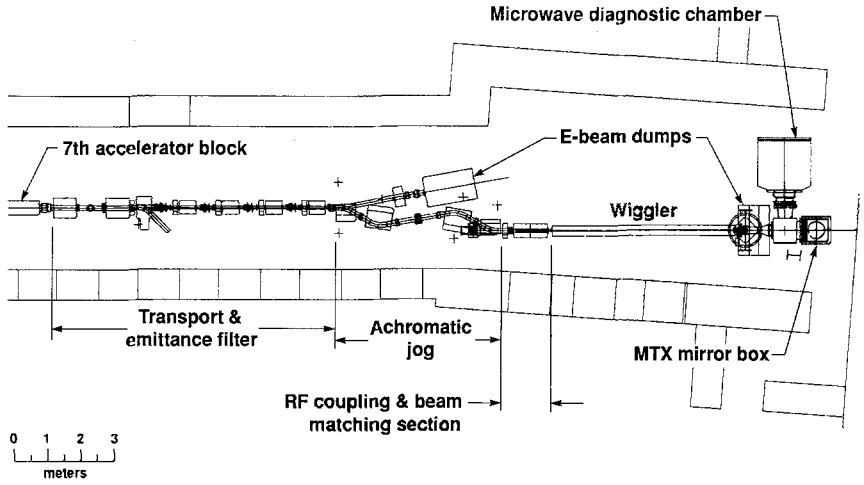

Fig. 8. Plan view of the 250 GHz FEL beamline.

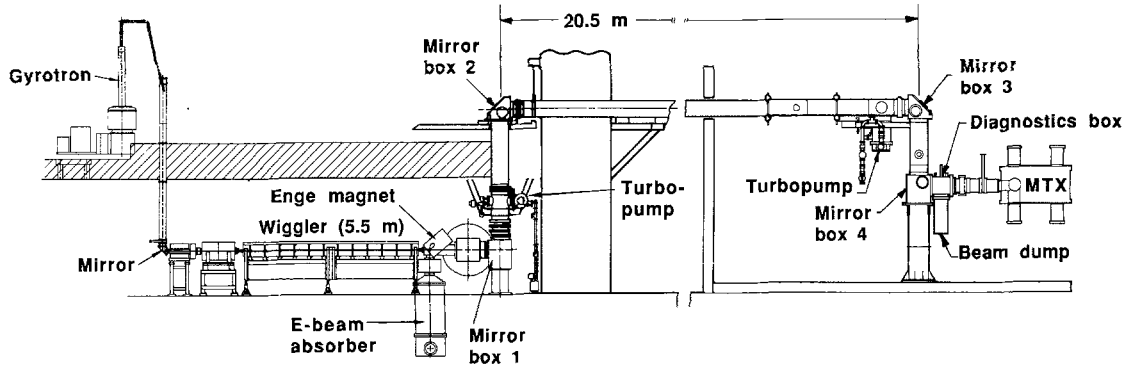

Fig. 9. Elevation view of the wiggler and microwave system for the MTX FEL.

Table II. Accelerator Requirements for IMP FEL with ETA-II Design Values

Parameter	IMP requirements	ETA-II design value
Energy (MeV)	10	10
Current (kA)	3	3
Brightness [10^8 A/(rad − m)^2]	1	20
PRF (kHz)	5	5
Pulse width flattop (ns)	50	50
Energy regulation (%)	1	0.4
Burst length (s)	0.5	30

Table III. ETA-II Initial Performance

Item	Value
Energy (MeV)	5.2
Current (kA) from injector	1.4
Pulse width (ns) FWHM	70
PRF (Hz)	1
Brightness [A/(rad − m)^2] through accelerator	6×10^8

through 15 m of wiggler without measurable loss using a fill factor that is comparable to that proposed for IMP. The upper limit on the electron beam loss is about 0.1% per meter in the wiggler wave guide. At this level, thermal loads are dominated by attenuation losses of the amplified microwave signal.

At the exit of the wiggler, the electron beam has a large (2:1) energy spread due to the FEL interaction. An

Table IV. ETA-II Performance Goals

Item	Value
Energy (MeV)	10
Current (kA)	3
Pulse width (ns)	
FWHM	70
Flat to 1%	50
PRF (Hz)	
Burst	5000
Average	100
Brightness [A/(rad − m)²]	2×10^9

Enge magnet is used to accommodate this energy spread and to magnetically "re-image" the beam from the FEL into a beam absorber (Fig. 8). For IMP, the beam absorber is a simple graphite mass using thermal inertia to absorb the enrgy during the 0.5-s heating pulse with subsequent cool-down between MTX shots.

Rf Coupling and Beam-Matching Sections. The beam-matching section is used to focus the electron beam into the wiggler to minimize any betatron motion that would degrade the FEL performance. To obtain the required circular equilibrium cross-section and waist condition at the wiggler entrance, two pairs of quadrupole doublets are located immediately in front of the wiggler.

The rf coupling section, located near the beamline-matching section, injects the input microwave signal colinearly with the electron beam. For the initial series of single-pulse experiments using the ELF wiggler, the input signal will be coupled into the wave guide as in the original ELF experiment.[18] A thin, 90-lpi wire mesh oriented at 45° in the beamline is used to reflect the master oscillator signal into the wiggler, while the electron beam passes through the mesh with only a small current loss and emittance growth.

For HAP operation, a method of coupling the input microwave signal that does not intercept the electron beam is required. Two methods are being studied. The baseline design for IMP specifies an achromatic jog (A-jog) to offset the axis of the accelerator from that of the wiggler by 70 cm. The A-jog would consist of four bending magnets: two to bend the beam through an angle of 40° and two for 30°. A quadrupole doublet would be required to match the beam into the A-jog, and a pair of quadrupole doublets to match it from the A-jog into the wiggler. With the A-jog, the microwave signal can be injected straight through the beam-matching section into the wiggler. To accomplish this, power is coupled from a gyrotron source (Fig. 9) into a free-space Gaussian mode. This signal is then reflected and focused by a 15.2-cm-diam mirror through return-current slits in the last bend of the A-jog in to the wiggler wave guide (Fig. 10). Diffraction of the microwave beam and other transmission losses result in an insertion loss of about 10 dB.

An alternative method that does not require an A-jog is desired to minimize costs. Several methods are being studied. In general, these methods involve an apertured reflector that is located within the beamline and that injects the microwave signal into the wave guide at a slightly oblique angle. The electron beam is transmitted through the aperture in the reflector with negligible loss. A design that limits the insertion loss to 8–10 db has been completed and is now the preferred alternative to an A-jog.

Wiggler Assembly. The requirements for the IMP wiggler are listed in Table V. The simultaneous requirements for high field and large tuning range, along with low pole-to-pole random field errors, present the major technical challenge. However, simulation models and prototype measurements show that these requirements can be met using a permanent-magnet laced electromagnet wiggler.

The present polepiece design for IMP uses a gap of 3.7 cm, representing an acceptable tradeoff of tuning range against access for cooling the wave guide. A conservative design involving low-carbon-steel poles is also used to minimize RMS wiggler errors. Simulations of the pole design predict a tuning range of over 50%.

The active length of the wiggler is 5.4 m, and it uses 27 separate power-supply channels, each of which will energize a two-period-long section. Each section is designed to produce no net steering and no net displacement regardless of field setting. This is accomplished by overlapping the ends of each section, with the number of coil turns on each pole in the proper ratios, a so-called "steering-free pattern." In addition, the steering-free excitation pattern prevents beam steering even when the beam energy is changing rather rapidly along the axis of the wiggler, as it will in IMP.

Detailed design on the IMP wiggler is in progress. A one-period-long magnet prototype (10-cm period) was constructed to verify the operating field levels, and the full 5.5-m wiggler will be built and tested in preparation for deployment on ETA-II in the fall of 1989. Prototypes of other wiggler designs have been completed and have performed as expected.

Until the high-field IMP wiggler is available, the initial MTX experiments will use the pulsed wiggler developed for the original ELF experiments. The pulse wiggler can produce peak magnetic fields on an axis of up to 5 kG for less than 1 ms. The 4-m-long wiggler is composed of specially shaped solenoids that provide a

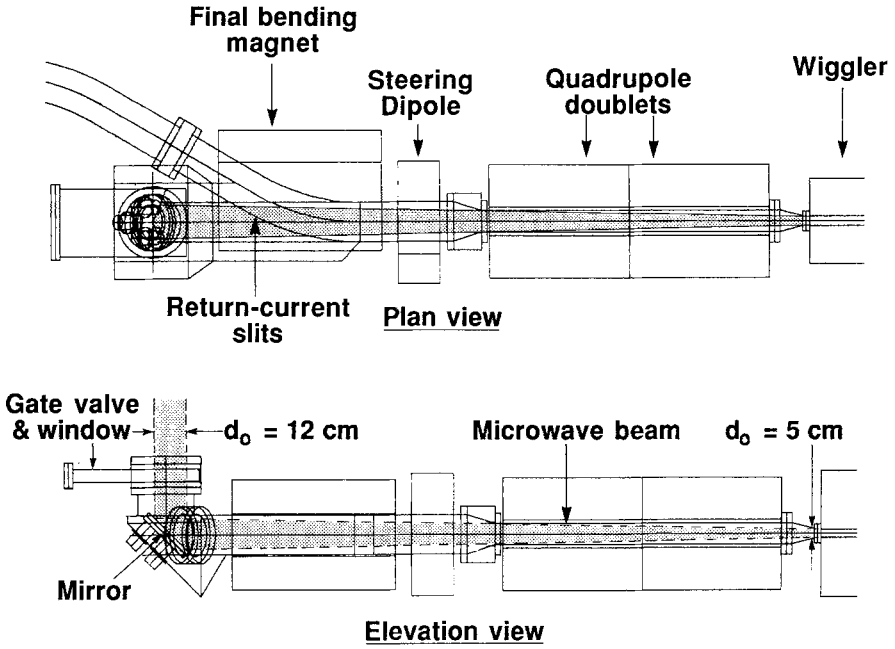

Fig. 10. Plan and elevation views of the section of the achromatic jog used to colinearly inject the electron beam and master oscillator signal into the wiggler.

Table V. Requirements for IMP FEL Wiggler at 250 GHz

Wiggler period	10 cm
Wiggler gap	4.0 cm
Peak field	4.7 kG
RMS wiggler errors	< 0.1%
B-field tuning range	> 37%

linearly polarized wiggler with a 9.8-cm period. Vertical focusing of the electron beam is provided by the natural focusing of the wiggler field. Horizontal focusing is provided by continuous quadrupoles with a field gradient of about 30 G/cm.

Focusing in both the vertical and horizontal planes in the new IMP wiggler will be provided by parabolically-curved magnet poles faces. However, in strongly tapered wigglers (such as IMP), the focusing force decreases at the lower magnetic fields, thereby increasing the beam size and placing a practical limit on the amount of taper.

Microwave System. The microwave system, shown schematically in Fig. 9, consists of the gyrotron (master oscillator), the rf coupler, the wiggler interaction wave guide, and the microwave transmission system to transport the FEL high-power output to MTX.

The 250-GHz master oscillator is a fixed-frequency gyrotron, operating at second harmonic. It uses a complex cavity and operates in the $TE_{11,2}$ mode. As for any IFEL master oscillator, the average power is low, about 200 W. The tube has been tested and produced 10 kW of peak power at 80 kV.

Two frequency-tuneable sources are being developed and may be deployed on MTX for testing if available. The first source, a step-tuneable gyrotron, was demonstrated at MIT to operate at the several-hundred-kW peak-power level and over frequencies from 130–240 GHz. MIT is investigating the ability to couple power from a step-tuneable gyrotron over a range of frequencies and modes using a single Vlasov coupler. The second source, a BWO gyrotron, is in an early research phase but represents a source that is potentially tuneable over a frequency range of 6–8% on a submillisecond timescale and that could operate at frequencies up to about 300 GHz.[19]

The handling and propagation of a high-power microwave beam is a major objective of MTX. High-power radiation is generated within the FEL interaction waveguide and is transported more than 30 m (Fig. 9) to MTX using a quasi-optical microwave transmission system.

The wiggler interaction wave guide is shown schematically in Fig. 11. The wave guide dimensions are

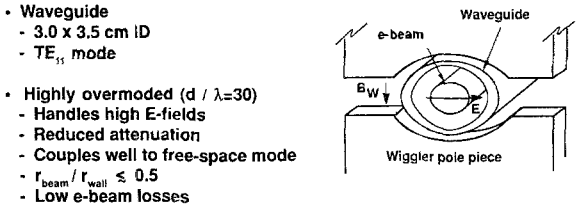

Fig. 11. Schematic of the FEL interaction waveguide for MTX.

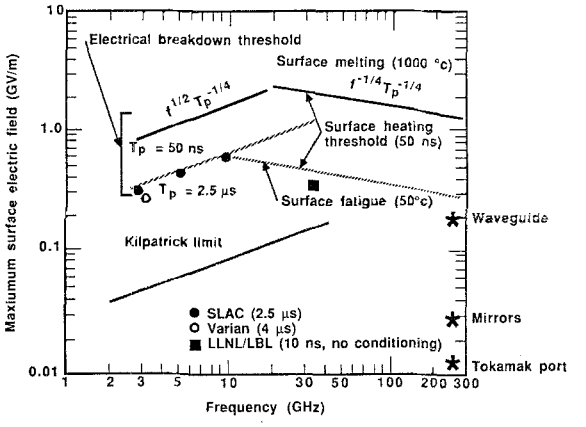

Fig. 12. Limits on surface electric fields for electrical breakdown and surface heating. Field strengths for components of the MTX FEL are noted.

chosen to minimize the cross-sectional area of the wave guide, thereby maximizing FEL gain, while keeping the linear beam fill factor to less than 50%. In general, microwave breakdown is not expected to be a major issue at the high frequencies and short 50-ns pulse length used in the experiment. Peak electric fields of 140 and 30 MV/m will occur in the wiggler wave guide and at the transmission system mirrors, respectively. These are well below the predicted breakdown threshold of 1–5 GV/m obtained from extrapolation of the Stanford Linear Accelerator Center (SLAC) and Varian data at 3–5 GHz, as shown in Fig. 12. Moreover, during ELF operation at 34.6 GHz, a threshold of 360 MV/m was measured for an unconditioned cavity. Similarly, calculations show that experimental parameters for IMP are well outside the range for multipactoring, either with or without a magnetic field.[20,21] Volume ionization and breakdown are not expected for vacuum pressures of interest to MTX since the length of the pulse is shorter than ionization time and plasma buildup is not possible.

At frequencies above about 30–50 GHz, transient surface heating places a lower limit on the allowed field strength than does microwave breakdown (Fig. 12). The temperature rise due to heating of the wave guide or mirror surfaces by the peak electric fields during the 50-ns pulse, if sufficiently large (>30–50°C), can produce surface strain that will result in microfracturing, and limit the useful lifetime of the surface. Within the wave guide, the energy depositon is about 0.07 J/cm^2 per pulse, which is about an order of magnitude below the measured damage threshold for an uncoated copper surface. The calculated margin based on temperature rise is somewhat less, about a factor of 2. The difference between the measured and calculated margin may be due to work hardening of the metal. In the transmission system, field strengths are well below surface heating thresholds. Thus, while not posing a significant issue for IMP operation, the data provided by IMP on surface heating will be useful in evaluating future higher peak-power FEL configurations.

As for the electron beam, issues related to handling the HAP of the microwave output are somewhat mitigated because of the relatively short heating pulse (0.5 s). The thermal load at the wave guide wall is dominated by attenuation of the megawatt-level microwave signal over the last meter of the wiggler. The maximum expected heat flux is about 300 W/cm^2. This load can be handled using thermal inertia during the heating pulse, with cooling between MTX shots.

The microwave transmission system uses four 43 × 58-cm aluminum mirrors to transport the 2 MW of average power from IMP to MTX. The transmission system was designed to preserved horizontal polarization of the FEL output, to keep the microwave power density well below mirror surface-heating damage thresholds, and to minimize transmission losses. As summarized in Table VI, the overall transmission efficiency is calculated to be over 92%. The major single power loss is at the first mirror in the transmission system (M1). Figure 13 shows the microwave profiles, calculated using a diffraction transport code, at M1 and at the MTX port. The power loss at M1 is caused by spillage of power in the

Table VI. Calculated Losses for MTX Microwave Transmission System

	Losses (%)
Mirror M1	3.7
Mirrors M2-M3	2.7
At MTX port	0.4
Dissipation	1.1
Total losses	7.9

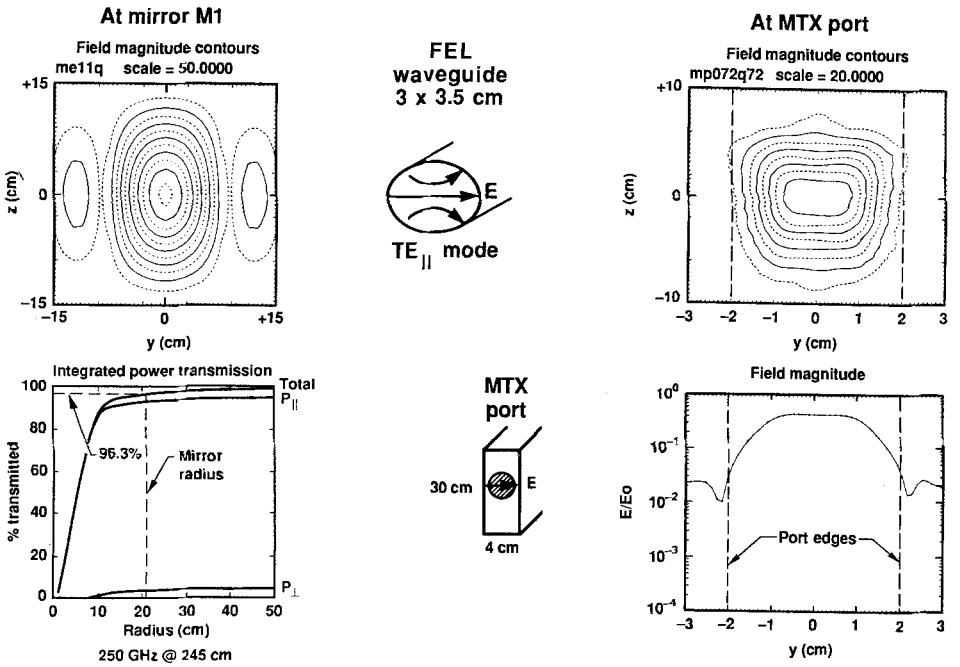

Fig. 13. Microwave field magnitude contours and radial profiles at the first mirror (M1) in the microwave transmission system for MTX and at the MTX port.

side lobes of the far-field radiation pattern of the FEL and represents a tradeoff against a practical mirror size and cost for MTX. The use of corrugated wave guide and the HE_{11} mode in the wiggler can reduce these side lobe losses.

The transmission system is windowless and maintained at a pressure of less than 1×10^{-6} Torr. The long conductance path between IMP and MTX provides a natural differential-pumping section to isolate the two vacuum systems.

2.2.4. *Phased Development to High Average Power*

High average power for IMP will be achieved in three phases, as reliable operation is tested initially at high PRF for short bursts, followed by longer pulse bursts up to 0.5 s. The operational parameters of the three phases are summarized in Table VII.

The first phase, scheduled for FY89, will involve single-pulse experiments at 140 GHz using the 4-m-long pulsed wiggler that was built for the original ELF experiment.[12–15] Figure 14 shows the results of simulations for this case. Because a higher beam energy and current are available from ETA-II, peak powers of over 2 GW can be produced. This is 13 dB higher than that measured on the original ELF experiment at 35 GHz. A 140-GHz extended-interaction oscillator (EIO) source will be used as the master oscillator and is expected to deliver about 50 W of signal into the wiggler.

Table VII. System Parameters for the Three Experimental Phases of the FEL for MTX

Parameter	Phase I	Phase II	Phase III
Beam			
Energy (MeV)	6	7.5	10
Current (kA)	2	2.5	3
Pulse width (ns)	20	35	50
PRF	0.5 Hz	5 kHz	5 kHz
Pulses/burst	1	50	2500
FEL			
Wiggler	ELF	IMP	IMP
Frequency (GHz)	140	140	250
Master oscillator	EIO	gyrotron	2ω gyrotron
TE_{01} power (GW)	2.4	3.8	11
rf Energy/shot (kJ)	0.05	6.6	1287

In these preliminary experiments, operation of the ELF wiggler is thermally limited to a single pulse every 2 s, effectively limiting MTX heating to one FEL pulse of about 50 J/shot. Nonetheless, these single-pulse ex-

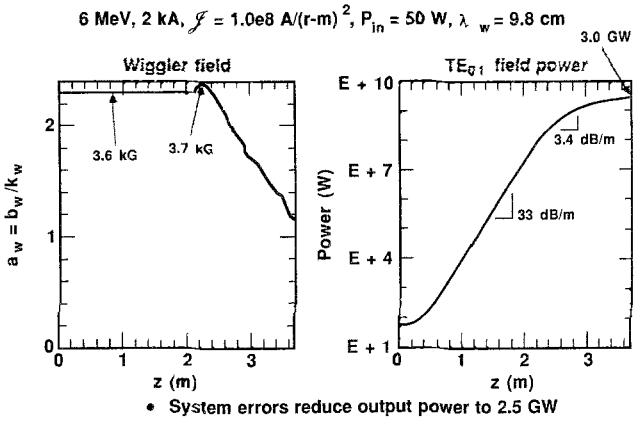

Fig. 14. Simulation results for the wiggler field and gain profile for the ELF wiggler.

periments will be very useful in achieving high-brightness electron beam transport, in studying FEL physics issues in this new operational regime, and in understanding how to efficiently transport the output of the FEL to the tokamak. In MTX, the single-pulse experiments will provide an initial measurement of the absorption of the intense microwave pulses without backscatter due to parametric instabilities.

The second phase of the experiments will occur in FY90 when the steady-state IMP wiggler and short-burst (10-ms) operation of ETA-II at a 5-kHz PRF are available. The FEL will produce a peak TE_{01} output power of over 3 GW at 140 GHz with a pulse width of 35 ns for a 10-ms burst at the 5-kHz repetition rate, i.e., about 50 pulses. A 140-GHz gyrotron capable of producing 25 kW of power (with about 1 kW input to the wiggler) will be used as the master oscillator. For these burst-mode operations, the IMP wiggler will be optimized for operation at 140 GHz, using 7.5-MeV beam energy. The wiggler magnetic field profile will be optimized for the taper at 140 GHz, and will thus differ from the 250-GHz profile. The FEL experiments will focus on the high-PRF operation and the IMP wiggler performance. The tokamak experiments will study plasma heating effects for heating duration times less than an energy confinement time and will provide quantitative measurements of the absorption and reflection of intense ECH pulses.

The third phase of the experiments will incorporate all the components for the HAP experiments and could occur in FY91. ETA-II will be upgraded for 10-MeV operation for the full 0.5-s shot duration. The FEL will operate at the design frequency of 250 GHz, with the master oscillator power input to the wiggler of about 500 W supplied by a second-harmonic gyrotron. The peak TE_{01} output power will be about 11 GW with a 50-ns pulse width at a 5-kHz repetition rate, supplying a maximum average power of about 2.5 MW for a shot duration of 0.5 s. The emphasis of the FEL experiments will be to demonstrate HAP FEL technology, while the tokamak experiments will concentrate on full-duration plasma heating. Experiments on profile control and current drive will also follow.

INITIAL DESIGNS FOR FUSION APPLICATIONS

3.1. Physics Design

The capability to predict the performance of FEL amplifiers operating in the regime where moderate space charge effects are important has been developed using the results of the experiments on ELF.[22] The success of these experiments and the demonstrated ability of numerical simulations in calculating the experimental results give confidence in the use of these tools to predict the performance of amplifiers at the 280- and 560-GHz frequencies that are suitable for fusion applications.[17,23,24] A description of the results used to select the baseline 10-MW FEL configuration follows. The FEL performance at several energies and for various electron beam currents was studied numerically, but results are shown only for the cases used in the baseline design.

3.1.1. Physics and Engineering Constraints

The electron beam energy selected must be between an upper and a lower bound. The upper bound is determined by the maximum magnetic field that the wiggler can produce for a given gap and period. Figure 15 shows that 5 kG is the maximum field that can be reasonably obtained for a 4-cm gap and a 10-cm period wiggler using permanent magnets and normal iron as the pole and yoke material.[25] The approximate FEL free-space synchronism condition for an rf wavelength λ and a wiggler period λ_ω is[26]

$$\lambda = \frac{\lambda_w}{2\gamma^2}\left(1 + a_w^2\right)$$

where γ = Lorentz factor, and a_ω = normalized vector potential. As shown in Fig. 16, the maximum energy that still satisfies the FEL synchronism condition with the 5-kG maximum field from Fig. 15 is about 12 MeV. The electron beam linear fill factor is required to be

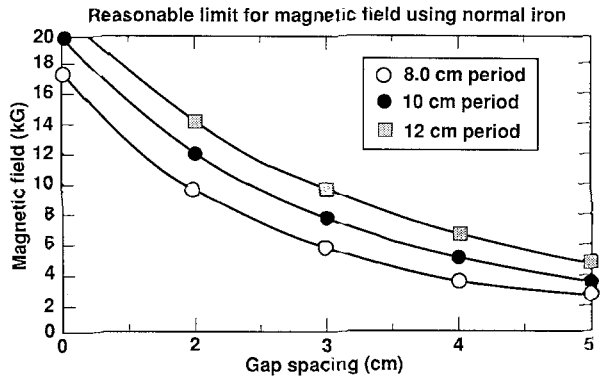

Fig. 15. Reasonable magnetic limits (Halbach limit) for wiggler period and gap using normal iron for the yoke and pole.

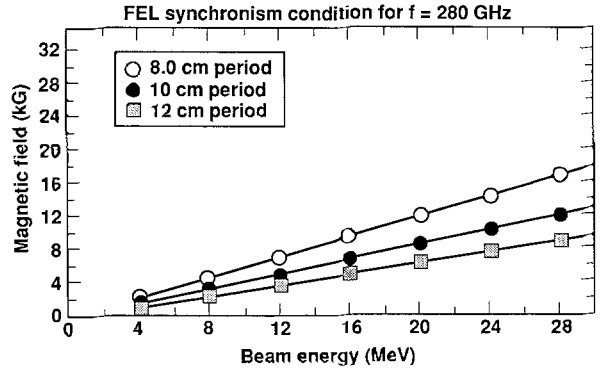

Fig. 16. Magnetic field required to satisfy the FEL synchronism equation as a function of energy and wiggler period.

about 50%, which places a lower limit on the wave guide dimensions. The linear fill factor is defined as the ratio of the beam linear dimension to the wave guide linear dimension in the same plane. Based on the expected amplitude of the electron beam wiggle, and on the beam size which is determined by emittance and wiggler focusing, a 3.5-cm circular wave guide is needed, which would require about a 4.0-cm gap.

The lower limit on the electron beam energy is set by one of two considerations. First, for fixed values of beam current and brightness, longitudinal space charge effects become more pronounced as the beam energy is decreased. These effects lower the peak gain at the fundamental while enhancing the relative gain at a lower frequency and also shift the peak gain away from FEL synchronism. Space charge also causes the electrons to spread more in the (γ,ψ) phase space, thus making it more difficult to trap electrons in the ponderomotive well and to keep them there when tapering the magnetic field. At some point, it becomes difficult to capture a large fraction of electrons in the ponderomotive well, tapering becomes ineffective, and the output peak power decreases.

The second consideration in setting a lower limit on the beam energy is the expected overall efficiency of the FEL in combination with the desired output power. If the peak power drops to some lower value, the FEL duty factor becomes too large for some of the systems in the accelerator power conditioning chain. In practice, the second consideration sets the lower limit on beam energy.

3.1.2. FEL Design with No Errors

The FEL interaction is modeled using the HE_{11} mode for microwaves in a circular corrugated wave guide. This mode is necessary due to excessive wall heating produced by the TE_{11} mode in a smooth-wall circular wave guide. The HE_{11} has a spatial distribution that is more peaked about the axis of the wave guide and produces less dissipation in the walls.

The wiggler constant magnetic field is set to maximize the exponential gain at the desired frequency. This optimization can be done by a series of code simulation runs to generate the appropriate output rf power contours as a function of frequency and field, or more simply, by calculating the power spectrum for various values of magnetic fields and choosing the magnetic field value that puts the peak gain at the desired frequency.

Next, the length of the untapered section is optimized by monitoring the evolution of the particle orbits in (γ,ψ) phase space. This optimization of the untapered wiggler section permits a buildup of the fundamental signal while keeping noise amplification to a minimum. Once tapering begins, the magnetic field is chosen to be at FEL synchronism. In the tapered region, the incremental gain at the fundamental is smaller than a lower frequencies, hence the requirement for a high signal-to-noise ratio going into the tapered section. The calculated profile for the magnetic field in the tapered section of the wiggler is determined using a synchronous tapering scheme that is suitable for FELs operating in the Compton regime. Because the electron beam radius grows as the field strength is decreased, the wiggler is truncated when the linear fill factor approaches 50%, which corresponds to about a 25% area fill factor. When the effects of errors are included, the linear and area fill factors increase faster than without errors.

Figure 17 shows an axial profile of the predicted

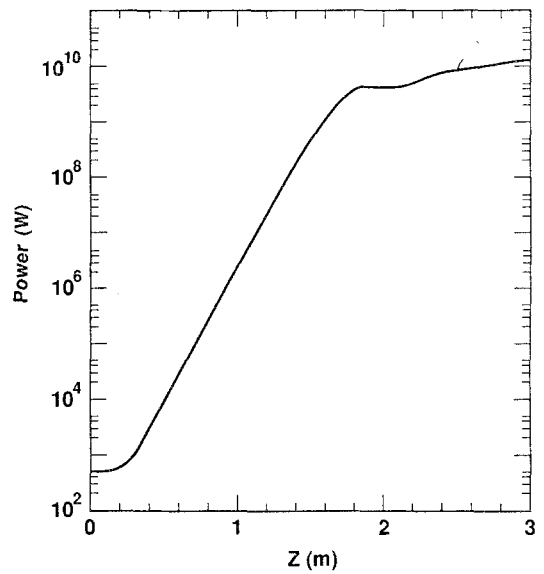

Fig. 17. HE_{11} power output vs. wiggler length showing exponential gain and linear gain after saturation at about 1.5 m.

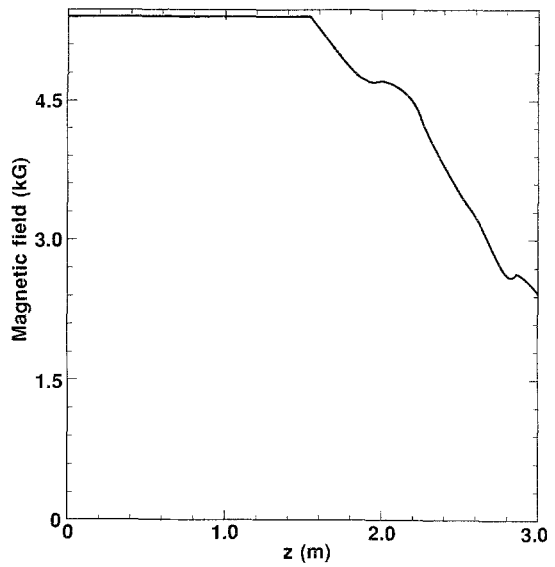

Fig. 18. Simulation results for the magnetic field vs. length for 280 GHz and an electron beam energy of 13 MeV.

HE_{11} peak power. With a beam energy of 13 MeV and a beam current of 3 kA, the HE_{11} power grows from the input level of 500 W at a rate of about 46 dB/m in the exponential gain region and attains a level of about 12 GW at the end of the 3-m-long wiggler. This corresponds to an extraction efficiency of 40% with 74% of the electrons trapped in the bucket. Figure 18 shows the wiggler magnetic field profile for this case. The constant field is 5.4 kG and the minimum field, limited by the fill factor, is 2.6 kG. Other runs have been made using different energies and currents. Results for the cases used for the baseline configuration selection are shown in Table VIII.

With a few minor exceptions, the 280- and 560-GHz configurations are the same. To obtain the same output power, the energy must be increased and the wiggler lengthened for the higher frequency case because of its lower extraction efficiency. The beam energy for the 280-GHz case will require a higher magnetic field than can be reached easily by a wiggler using normal iron.

3.1.3. FEL Design with Errors

The FEL performance shown in Table VIII assumes that the parameters are at their optimum values with no alignment or wiggler errors, no beam displacement, no energy sweep, and the full rated beam current. Such a situation is highly unlikely in the real world. Calculations were made in which errors were systematically introduced, to determine the acceptable ranges for these errors. Using the wiggler profile determined for the no-error case, the following parameters were varied: electron beam current, master oscillator power, beam energy sweep, beam displacement, and random wiggler errors.

For each case, the variable value was noted when the peak output power dropped to 80% of its no-error

Table VIII. Results for Baseline Cases[a]

	560 GHz	280 GHz
Beam parameters		
Energy (MeV)	15	13
Current (kA)	3	3
Brightness [A/(rad − m)²]	10^8	10^8
Input microwave power (W)	500	500
Wiggler parameters		
Period (cm)	10	10
Gap (cm)	4	4
Length (m)	4	3
Constant magnetic field (kG)	4.3	5.4
Peak magnetic field (kG)	4.3	5.4
Minimum magnetic field (kG)	1.7	2.6
Waveguide diameter (cm)	3.5	3.5
Results		
HE_{11} output power (GW)	17	16
Trapping efficiency (%)	65	74
Extraction efficiency (%)	37	40

[a] No errors.

case and also when the linear fill factor grew above 50%. Figures 19 and 20 shows samples of the result for one of these runs when only wiggle-plane displacement was considered. In other calculations, errors were combined to determine the total effect on performance. It was determined that the error limits were set by the constraint on the fill factor. The results are shown in Table IX.

Table X shows the FEL performance when these combined errors are included in the calculations. The no-error results are shown in parentheses for reference.

The large drop in the output power for the 560-GHz case was due to a +1% positive beam energy sweep.

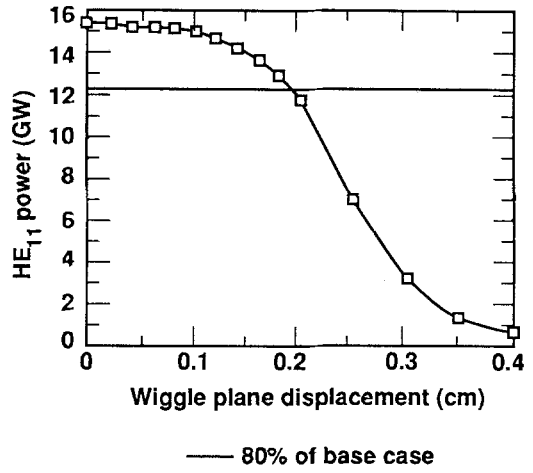

Fig. 19. HE_{11} power out vs. wiggle plane displacement from electron beam centerline.

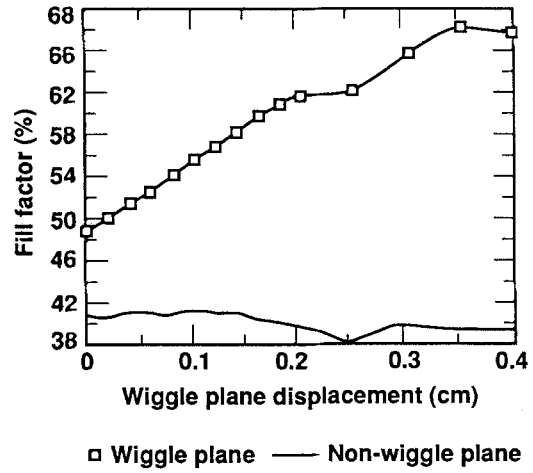

Fig. 20. Fill factor for wiggle and nonwiggle planes vs. wiggle plane displacement from the electron beam centerline.

Table IX. Error Limits for Combined Errors

RMS wiggler error (%)	<0.1
Wiggle plane beam displacement (cm)	<0.1
Nonwiggle plane beam displacement (cm)	<0.1
Beam energy sweep (%)	$< \pm 1$

Table X. Predicted Performance with Combined Errors[a]

	560 GHz	280 GHz
HE_{11} output power (GW)	10(17)	14(16)
Extraction efficiency (%)	23(37)	35(40)
Trapping efficiency (%)	28(65)	61(74)
Linear beam fill factor (%)	60(50)	55(50)

[a] No-error results are shown in parentheses.

This drop would be unacceptable and would require energy regulation to better than 1% during the pulse. Within other FEL programs at LLNL the requirements for allowed errors are more stringent than the above values. If these lower error limits are assumed, the peak power for both 280 and 560 GHz cases will only decrease by about 2%.

3.1.4. Conclusions

A beam energy and current was selected to provide about 17 GW of peak power if no errors are assumed. The 280- and 560-GHZ configurations differ only slightly. If it is assumed that the more stringent error requirements of other programs are met, this power would be expected to decrease by only about 2%. An output power of 14 GW, which was required for the baseline configuration, gives a margin of about 20% for power based on these predictions of FEL performance.

3.2. Methodology of Selection and Design

A methodology was developed to design and cost free-electron laser sources. A trade studies group has written algorithms that size and cost components and/or sub-assemblies. These algorithms are based on input from design teams, and their accuracy was verified with vendor bids where possible. Figure 21 shows the information flow for arriving at a final cost estimate of a FEL. The top requirements of frequency, peak or average power, run time, and other specific items are input. The peak

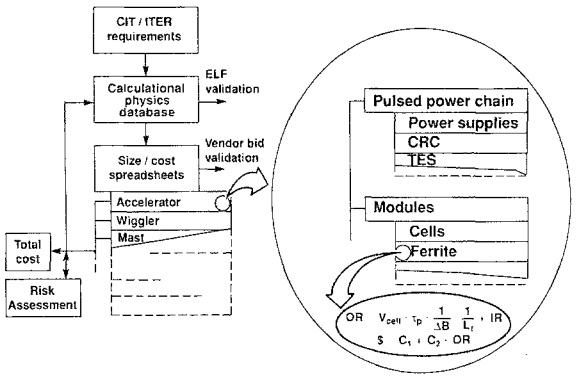

Fig. 21. Diagram showing the information flow to cost an FEL. Also shown, as an example, is an algorithm to cost the accelerator ferrite.

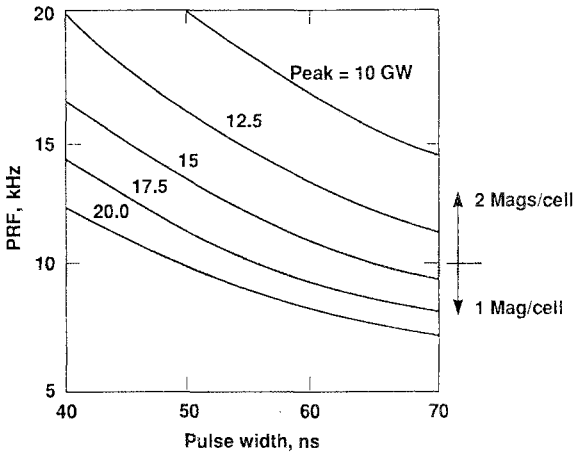

Fig. 22. Diagram showing the number of pulsed power chains per cell with PRF and pulse width for various peak powers.

power required based upon the allowable duty factor is determined. Our calculational database is checked to determine the electron beam energy and current necessary to produce the peak power. From the database, the length of the wiggler is also obtained.

For each major element of the FEL, algorithms were written that size and cost most of the components. Figure 21 shows, as an example, an algorithm for the accelerator ferrite. The ferrite outside radius is based on several variables which are shown in the figure. The ferrite is then costed as a fixed amount plus a constant times the outer radius. A commercially available spreadsheet is used for this calculation, with more than 100 components or sub-assemblies individually sized and costed.

Since the accelerator is the major expense of this system, its costs were minimized during this study. As a result of earlier work, limits for some of the components and sub-assemblies were determined, and a risk assessment of the extremes of these limits was completed. Figure 22 shows the effect of the limit of PRF $\leq$ 10 kHz and $\leq$1200 J/pulse for the magnetic compressor. If the peak power out of the wiggler is greater than about 14 GW and the pulse width is 70 ns or larger, only one power conditioning chain is required per cell. If the peak power is less than 14 GW, two power conditioning chains per cell must be multiplexed to get the duty factor required. Each chain would be running at one-half the required PRF while the cells operated at the proper PRF. Figure 23 shows the effect on costs vs. peak power for five cases. For each case, the energy needed to obtain the required peak power, the number of power conditioning chains, and the number of power supplies per chain were determined. These values were input into the spreadsheet, and the total cost of the accelerator was calculated. Figure 23 shows that the least expensive case,

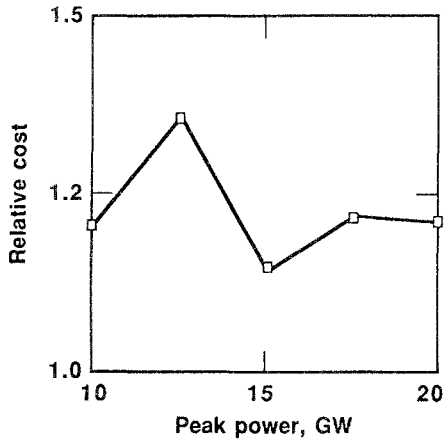

Fig. 23. Relative accelerator costs for five cases of increasing peak power.

of the five considered for 280 GHz, was an accelerator operating at about 15 MeV, 3 kA, 70-ns flattop pulse width, one power conditioning chain per cell, and both the power conditioning chains and the cells running at 10 kHz. A later run indicated the cheapest configuration was at 13 MeV. For this case, multiplexing is not needed, which is cheaper and reduces the risk.

3.3. Discussion of Designs

3.3.1. Requirements

Table XI shows the present top-level requirements for the next generation of fusion machines that could use FELs to provide electron cyclotron heating.

Table XI. Top-Level Requirements for Fusion Machines

Item	CIT	ITER
Input power (MW)	10	10–30
Frequency (GHz)		280
First	200–280	
Second	400–560	
Time on (s)	10	Steady-state
Shots/hr	4	TBD
Tuneability		
Fast (ms)	N/A	6–8%
Slow (s)	N/A	20%
Schedule	1991, demo. tech. 1994 installed	1991, demo. tech. 2000 installed

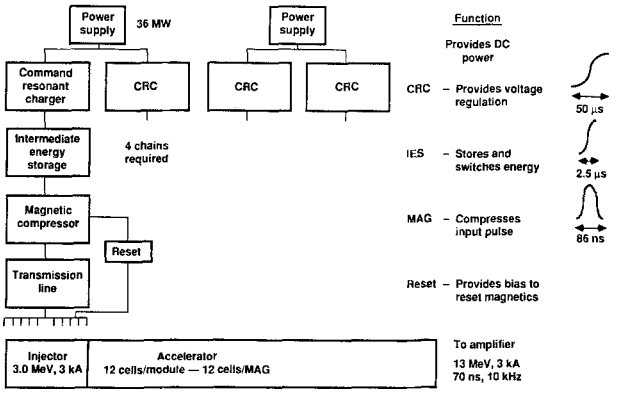

Fig. 24. Schematic of accelerator showing pulsed power chains and the function of each sub-assembly.

Two of the requirements of Table XI change the configuration of the baseline 280-GHz FEL. The first is the frequency required. As discussed earlier, the 560-GHz case requires more energy in the electron beam to produce the same peak power as the 280-GHz case. The ITER requirement for a continuously operating FEL affects the accelerator cooling and the electron beam absorber design. The absorber must be designed to remove the energy in real time as opposed to absorbing it in a material and removing it between shots.

3.3.2. 280-GHz Design

Figure 1 shows a schematic of the baseline configuration that produces 10 MW of average power at 280 GHz. Specifics of some of the elements are discussed here.

Accelerator. Using calculated results and the cost tradeoff, an accelerator was selected with the following parameters: energy = 13 MeV, current = 3 kA, volts/cell = 250 kV, flattop = 70 ns, PRF, max. = 10 kHz, brightness = 2×10^9 A/(rad-m)^2, cells/MAG = 14, MAG J/pulse = 1150 J, number of chains = 4, and power required = 85 MW. Figure 24, a schematic of the baseline accelerator, shows the function of the major subsystems.

The power conditioning chain was limited to a maximum PRF of 10 kHz. In addition, the maximum FWHM (full width half maximum) pulse width is limited to 100 ns and the maximum J/pulse out of a magnetic compressor to 1200. These limits were determined as a result of a risk assessment completed for another program. The same limits were used for this design to minimize the engineering design effort and risks for the system.

The accelerator cell ferrite selected is 1.27-cm thick. Figure 25 shows the run time vs. PRF for uncooled ferrite of any thickness. At a PRF of 10 kHz, the ferrite temperature does not increase to the limit of 50°C for a run time of less than about 30 s. Figure 26 shows that with the baseline thickness and a reasonable film coefficient, the cool-down time is about 10 min. This allows about four 30-s shots per hour.

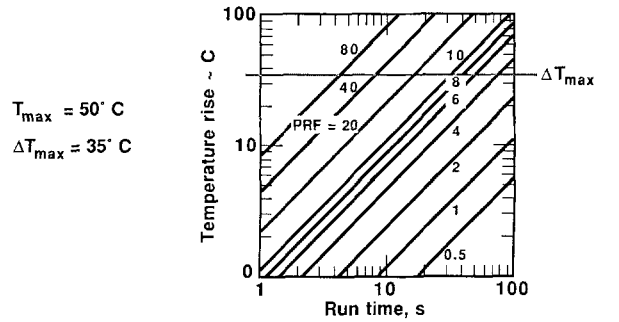

Fig. 25. Uncooled accelerator ferrite temperature rise vs. run time and PRF.

In addition to the ferrite heating during a run, Metglas in the magnetic compressors will heat as a result of losses. Figure 27 shows that for a PRF of 10 kHz and a temperature rise limit of 50°C, the run time can be about 11 s.[27] Methods for cooling the Metglas are being evaluated, and experiments will be performed to verify the calculations. Since the run time required for CIT is 10 s, the power conditioning chain and the ferrite can run uncooled.

For ITER, the ferrite and the Metglas must be cooled continuously. Figure 28 shows the steady-state temperatures expected for various thicknesses of ferrite and

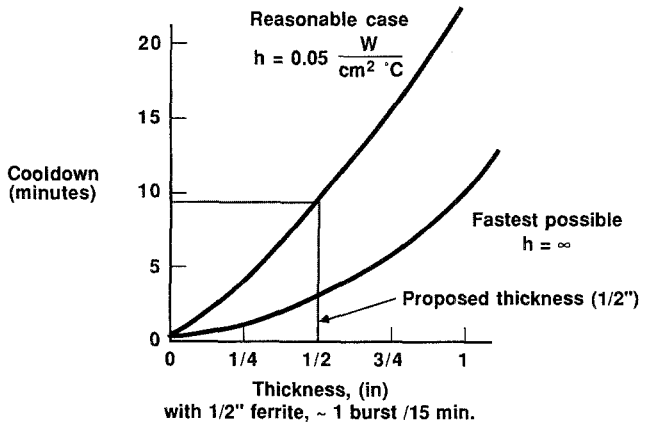

Fig. 26. Cool-down time vs. ferrite thickness for two cases of surface film heat transfer coefficient.

$$T_{max} \sim \frac{(E*PRF)\left(\frac{L}{2}\right)^2}{2k} + \frac{(E*PRF)\left(\frac{L}{2}\right)}{h} + T_{Fluid}$$

Where: E = energy/pulse/vol
k = Thermal conductivity
h = Ferrite wall, fluid film coefficient
L = Ferrite thickness

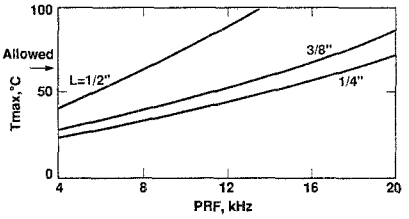

k = 0.033 W/cm-°c
h = 0.05 W/cm² -°c
E = 360 J/cm³/pulse

Fig. 28. Steady-state temperature of accelerator ferrite vs. PRF and thickness.

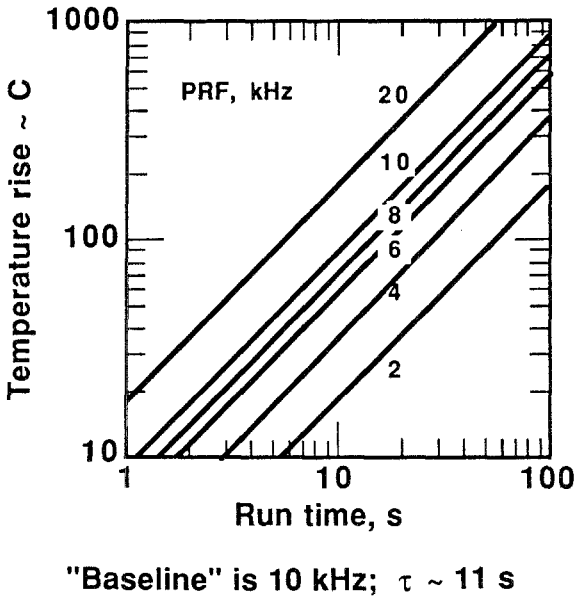

Fig. 27. Temperature rise of uncooled MAG metglass vs. run time and PRF.

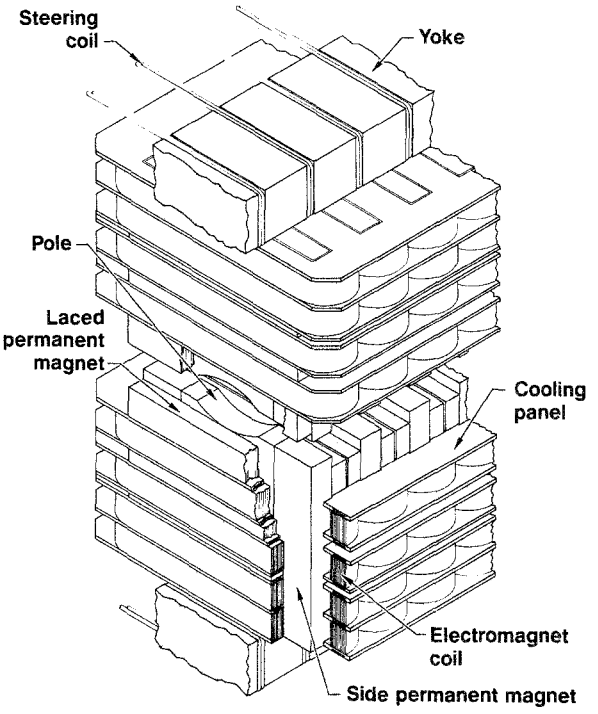

Fig. 29. A wiggler pole design using both side and laced permanent magnets and four electromagnet coils.

PRFs. At 10 kHz, a 1.27-cm-thick ferrite would be acceptable, but a thinner disk would be desirable. A thickness of ferrite less than the 1.27 cm for the ITER design would be specified to provide a design margin.

Wiggler. Figure 29 shows a layout of a laced wiggler that uses permanent magnets and electromagnets to obtain the field in the gap. A one-pole prototype of this configuration using iron as the bus and pole material was constructed. A magnetic field corresponding to the Halbach limit for the specified gap/period was reached. Although the Halbach limit was determined for a different configuration, it is excellent measure of the degree of difficulty of obtaining specific field levels for a design which uses normal iron in the pole. Calculations were made using the LACED code to determine the maximum field that could be obtained as a function of the bus and pole.[28] Using this field value, the maximum electron

beam energy that can be used for a specific frequency and still match the FEL synchronism condition can be calculated. These results are shown in Fig. 30 for a design using iron that will reach the Halbach limit in the gap and another material (vanadium Permendur) that would allow a design that woud reach reach 1.5 times the Halbach limit in the gap. For the gap and period selected, the maximum energy usable at 280 GHz and with iron is about 11 MeV; with a material such as vanadium Permendur, about 17 MeV is allowed. The accelerator costs are a minimum with a peak power out of the wiggler of about 14 GW, which requires a beam energy of 13 MeV. Therefore, vanadium Permendur must be used as the pole material in the wiggler

The temperature rise was estimated for a smooth copper 3.25-cm-inside-diameter waveguide operating at 280 GHz for the TE_{11} mode. This temperature increase is due to power generated by rf currents in the wave guide wall. An attenuation enhnacement factor of 3 for losses was used. This factor of 3 over the theoretical is a result of surface roughness, high wall average temperature, and an anomalous skin effect. The heating of the guide during the pulse was modeled as a semi-infinite slab with heat flux at the boundary. Table XII shows the temperature rise for various wave guide materials at different frequencies.[29] A peak of 10 GW, a pulse width of 70 ns, and a 3.25-cm guide were assumed for these calculations.

The case of one-dimensional strain was assumed to estimate the allowable temperature surface rise on the surface of the rapidly heated material. If typical copper properties at room temperature are used, the temperture

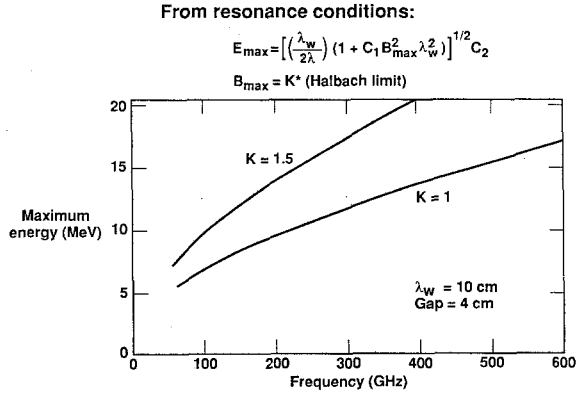

Fig. 30. Maximum energy vs. frequency that satisfies the resonance conditions for two maximum magnetic fields at a wiggler period of 10 cm. *K*, a multiple of the Halbach limit, represents the increase of the maximum saturation field allowed in the pole material compared to normal iron.

rise should be less than 30°C to give a fatigue in life of greater 10^8 cycles. As shown in Table XII, for the cases considered, none of the materials appear to be acceptable as wave guide choices. In addtion, the average heat flux removal rate would be serveral kW/cm^2 over the last meter of the wave guide. Although this type of heat flux can be handled with subcooled nucleate boiling, the design would be high risk. Therefore, the use of a corrugated wave guide in the wiggler is specified.

If a corrugated wave guide is used, the wall heat loading will be reduced by about a factor of 800–900.[30] With this large reduction in heating, the peak power can be increased up to the 14-GW level, which is required for the configuration selected for the baseline. Arcing and multipactoring were examined for the corrugated wave guide. For a 280-GHz guide, the rf field caculated at the corrugation is about 30 kV/cm. The rf breakdown threshold is about 58,000 kV/cm for the case considered, so no arcing should occur.[21] For multipactoring considerations, the product of frequency and groove dimension and the product and electric field and groove dimension were calculated. The resuls were far outside the region where multipactoring would be a problem.[20]

The variables for the wiggler baseline were specified as: gap = 4.0 cm, period = 10 cm, length = 3 m, pole material = vanadium Permendur, field = 5.7 kG, and wave guide = corrugated, copper 3.5-cm ID.

Electron Beam Transport and Absorber. Included in the beam transport system are the usual quadrupoles, dipoles, and steering coils. The electron beam is steered into the absorber by an Enge magnet, which turns electrons with a wide energy spread by the same amount. This type of magnet will be used on MTX. The electron beam transport also contains diagnostics that will duplicate those planned for present experiments. Within this element, no components have even moderate risks of operation.

For beam-on times of about 5 s or less, an appropriate mass of material can be used to absorb the energy

Table XII. Temperature Rise, °C, for certain Materials vs. Frequency

	Frequency (GHz)		
Material	140	250	560
Copper	63.6	84.6	126.4
CuO.4BeNi	83.2	111.2	166.3
C15715	71.1	95.2	142.1
Aluminum	122.0	162.8	243.9
Al 6061-T6	163.0	217.6	325.2

in the electron beam; the heat will be removed between shots. An actively cooled absorber must be used when the run time is 5 s or more. A conceptual design of a water-cooled absorber based on a SLAC configuration has been completed.[31] For an ITER design, 10-cm-diam thin-walled (2-mm) aluminum tubes cooled by high-velocity water which also absorbs the remaining energy in the electrons would be used. This baseline configuration requires an electron beam area of about 4000 cm^2 with the water velocity at the aluminum/water boundary being 10 m/s. This gives a safety factor of about 2.2 on the critical heat flux. The stress in the tubes for several end restraint conditions was below the elastic limit at the operating temperature; therefore, a long fatigue life would be expected. Two rows each of 12 tubes side by side are required to stop the electrons completely.

Microwave Driver and Transport System. A program is ongoing to develop a tuneable master oscillator. The BWO was designed to operate at 250 GHz, tuneable to ± 3% with an output of 10 kW. The basic design is described elsewhere.[19] A step-tuneable gyrotron is presently available for 250 GHz and can serve as a backup.

Figure 31 shows a layout of a possible microwave transport system for CIT. This quasi-optical design is based on the present configuration chosen for MTX. The losses at each mirror and the surface temperature rise during each pulse must be limited. The mirror diameter must be large enough so the loss is low over the longest path. From the layout, the longest path was determined to be 24.4 m. A Gaussian beam was assumed, and the mirror radius is calculated so that the power at the edge is $1/e$ of the maximum. For the 280-GHz case, the radius is 6.45 cm. The loss is limited by making the actual diameter greater than or equal to six times the above radius, giving a 39-cm diameter for a 280-GHz mirror and a 27-cm diameter for a 560-GHz mirror. Note that a mirror designed for 280 GHz will transport 580 GHz with lower losses.

To eliminate surface fatigue of the copper mirrors, the energy absorbed per pulse should not be sufficient to increase the temperature 30°C or more. This temperature rise can be avoided for a 14-GW, 70-ns FWHM pulse if the minimum radius is 5.3 cm at 280 GHz and 6.3 cm at 560 GHz. Both of these are less than the 6.45-cm radius required for low loss, so the mirrors should have a long life.

3.3.3. 560-GHz Design

The 560-GHz case is similar to the 280-GHz design, except that a higher beam energy is required and the wiggler is longer. The extraction efficiency of the 560-GHz case is below that of the 280-GHz case; therefore, higher beam energy is required to extract the same amount of peak power at 560 GHz. This higher energy will affect the absorber design but will have little effect on the other elements. The cost of the beam transport system power supplies is estimated based on available units. Off-the-shelf units can supply the increased power required for the higher energy beam transport. A longer wiggler is required for this case, but the magnetic field is slightly lower. A master oscillator must be designed to operate at this frequency, and it will not be tuneable.

Since the extraction efficiency is lower for 560 than for 280 GHz, the wall-plug power must increase for the same average output power.

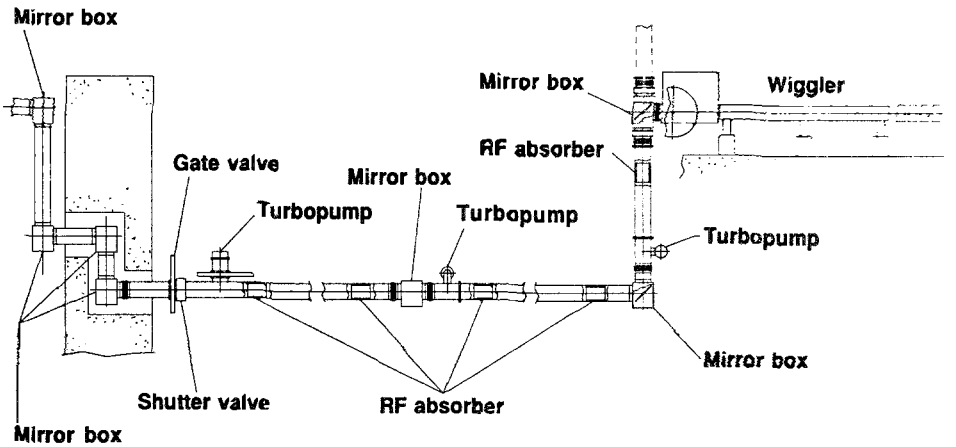

Fig. 31. Schematic of microwave transmission system from the FEL to the entrance of a fusion machine.

3.3.4. Facilities

Figures 32 and 33 show an elevation and plan view, respectively, of the 280-GHz configuration as it would be installed in the CIT facility at Princeton Plasma Physics Laboratory (PPPL). This illustrates the footprint required for a 10-MW unit. The size of the CIT components was based on the present MTX design. If the facility configuration dictates, the accelerator and wiggler can be placed side by side, which reduces the overall length but increases the width of the basic system.

The 280-GHz design will require about 90 MW of wall-plug power, and the 560-GHz configuration will require about 111 MW to produce the 10 MW of average power.

3.3.5. Radiation

The diffusion of tritium down the microwave transport system into the FEL was considered. A microwave window was not specified for the baseline configuration because FEL pressure requirements are not severe and, in any case, one must always provide for failure of a

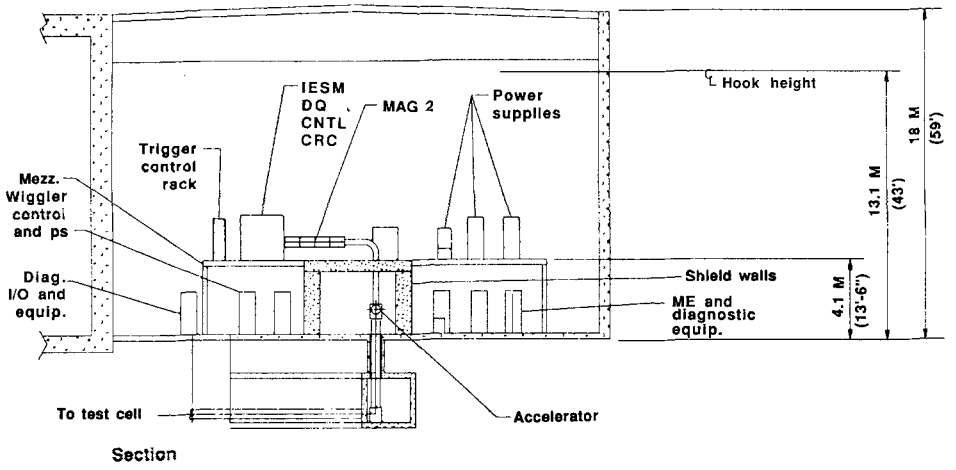

Fig. 32. Elevation view of a 10-MW FEL installed in the TFTR mock-up room.

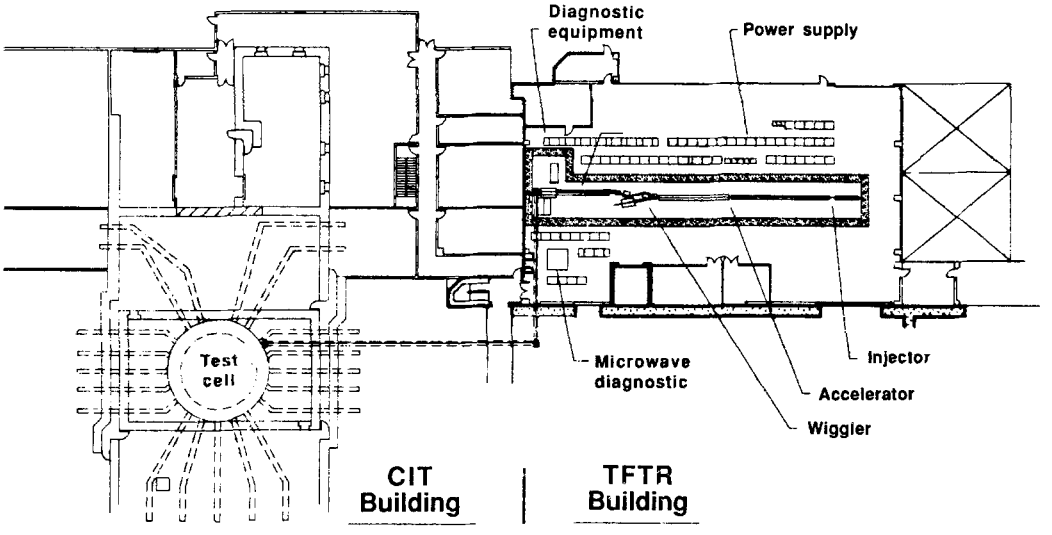

Fig. 33. Plan view of a 10-MW FEL installed in the TFTR mock-up room.

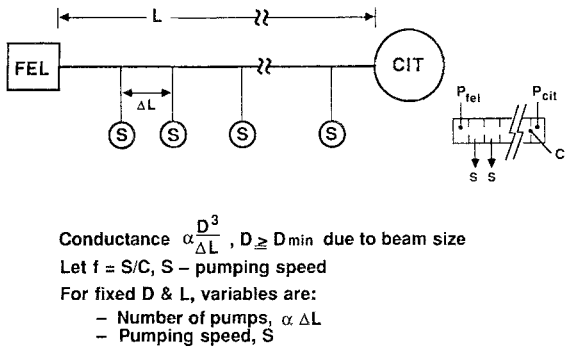

Fig. 34. Schematic showing the model used to estimate the tritium flow to the FEL.

Table XIII. Tritium Pressure at the FEL for 10^{-4} Torr Tritium Pressure at CIT[a]

	Number of pumps (pressure = 10^{-6} Torr)		
Pump speed/conductance	4	6	8
0.25	22	6	3.1
0.5	9.4	2.3	0.59
0.75	4.9	0.9	0.17
1.0	2.9	0.43	0.06
Conductance between pumps, 1/s	1200	2000	2700

[a] Pipe diameter is 50 cm, total length = 90 m.

tritium barrier if used. The schematic shown in Fig. 34 was used to calculate the amount of tritium that would reach the FEL per shot. It was assumed that a valve would be opened immediately prior to the shot and closed as soon as the FEL was turned off.

The conductance of a pipe for molecular flow is proportional to the cube of the diameter and the inverse of the length. A pumping station was placed every ΔL meters, as shown on Fig. 34, and its capacity was assumed to be a fraction of the incremental conductance. Table XIII shows the results for various ratios of pumping capacity to conductance.

The tritium pressure at the FEL should be down to about 10^{-6} Torr. Either six pumps with a pumping capacity of 75% of the incremental pipe conductance or eight pumps with about 30% of the pipe conductance will be sufficient to reduce the assumed CIT 10^{-4} Torr tritium pressure to 10^{-6} Torr. Available pumps can easily obtain pumping speeds of 1000 l/s for tritium; therefore, the reduction of 100 in pressure does not appear difficult to achieve.

To determine the maximum diffusion of tritium into the FEL, it was assumed that there was no pumping during a 10-s shot. The conductance of the 50-cm-diam, 90-m-long pipe was about 400 l/s. The partial pressure of tritium was assumed to be 10^{-4} Torr and the pressure at the FEL was 0. For this case, the amount of tritium diffusing to the FEL in 10 s was about 0.4 Torr·ℓ. The total volume in the FEL without the microwave transport was estimated to be about 750 ℓ. If there is an up-to-air accident, the percentage of hydrogen in the mixture is far below the lower explosion limit of 4%.

The 0.4 Torr·ℓ represents about 1.5 curies of activity. When compared to the total inventory in the fusion machines, this amount is not large. The FEL rough vacuum must be connected to the same tritium-processing system as all other roughing pumps. In addition, if six to eight pumps of a reasonable size are used, the numbers calculated here will be down by a factor of 100. If the partial pressure of tritium in CIT is less than that assumed, the amount diffusing to the FEL also will be less. These calculations indicate that the tritium can be pumped in the microwave transport pipe prior to the last concrete wall before the FEL. It is suggested that a high-capacity cryopump be placed near the fusion machine in the transport line, which could also be used to regenerate other pumps if necessary.

3.4. Frequency Option

Figure 35 shows a possible configuration that would inject two rf frequencies into a fusion machine for a small increase in cost. Figure 30 shows the maximum energy that is usable for a given frequency and wiggler material choice. If the electron beam is switched alternately to each of the wiggler lines and the wiggler fields are set to that required by the FEL synchronism condi-

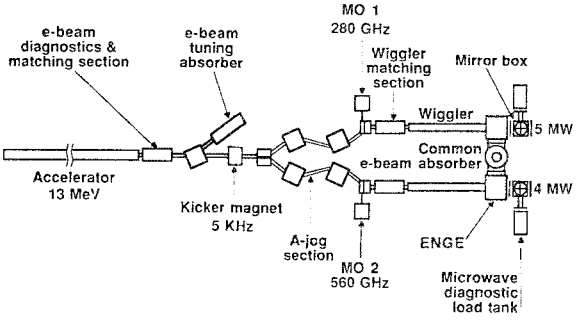

Fig. 35. Schematic of an FEL operating at two different frequencies, 280 and 560 GHz, with only one accelerator.

tion, power at two frequencies can be extracted. As an example, an accelerator operating at kHz with the beam switched between one wiggler tuned for 280 GHz and the other for 560 GHz is illustrated. For the example of a 13-MeV accelerator, the 280-GHz line would produce about 5 MW and the 560-GHz line about 4 MW. Separate master oscillators must be provided for each wiggler line.

4. CONCLUSIONS

Past FEL experiments at LLNL have achieved high peak power at 35 and 140 GHz. Numerical simulation results have matched the experimental data sufficiently well to give confidence in our ability to design FELs operating in the microwave regime.

Planned tests on MTX will reach higher peak power and, more important, higher average power at 140 and 250 GHz. Both the physics and the technology relevant to a CIT design will be demonstrated. In addition, tests are ongoing on various test stands to advance the technology for increased component and system performance.

An FEL configuration has been selected for ECH applications on fusion machines. This configuration minimizes costs and risks, because it is based upon technology to be developed for other LLNL programs. Present and planned future efforts should lead to the development of a microwave FEL for electron cyclotron heating purposes by the early 1990's.

ACKNOWLEDGMENT

This work was performed under the auspices of the U.S. Department of Energy by Lawrence Livermore National Laboratory under Contract W-7405-Eng-48.

REFERENCES

1. K. I. Thomassen, (1988). Millimeter wave tokamak heating and current drive with a high power free-electron-laser. *Plasma Phys. Cont. Fusion,* **30**, 57.
2. W. M. Nevins, T. D. Rognlien, and B. I. Cohen, (1987). Nonlinear absorption of intense microwave pulses. *Phys. Rev. Lett.,* **59**, 60.
3. W. M. Nevins, (1986). Private communication; K. I. Thomassen, ed. Free-electron laser experiments in Alcator-C. LLL-Prop-002, Lawrence Livermore National Laboratory, July 1986.
4. T. D. Rognlien, (1983). Frequency splitting and collisional decorrelation for removing superadiabatic barriers in ECRH experiments. *Nucl. Fusion,* **23**, 163.
5. T. D. Rognlien, Private communication.
6. A. Cardinali, M. Lontano, and A. M. Sergeev, (1989). Dynamical self-focusing of the high-power FEL radiation in a magnetized plasma. *Phys. Fluids,* **B1**, 901.
7. B. I. Cohen, *et al.* (1988). Plasma heating and current drive using intense, pulsed microwaves. Proceedings International Workshop on Theory of Fusion Plasma, Chexbres, Switzerland, October 3–7.
8. C. E. Max, (1976). Strong focusing due to the ponderomotive force in plasmas. *Phys. Fluids*, **19**, 74.
9. M. Porkolab and B. I. Cohen, (1988). Parametric instabilities associated with intense electron cyclotron heating in the MTX tokamak. *Nucl. Fusion*, **28**, 239.
10. B. Hui, E. Ott, P. T. Bonoli, and P. N. Guzdar, (1981). Scattering of electron cyclotron resonance heating waves by density fluctuations in tokamak plasmas. *Nucl. Fusion*, **21**, 339.
11. E. Ott, B. Hui, and K. R. Chu, (1980). Theory of electron cyclotron heating of tokamak plasmas. *Phys. Fluids*, **23**, 1031.
12. T. J. Orzechowski, B. R. Anderson, J. C. Clark, W. M. Fawley, A. C. Paul, D. Prosnitz, E. T. Scharlemann, and S. M. Yarema, (1986). High-efficiency extraction of microwave radiation from a tapered-wiggler free electron laser. *Phys Rev. Lett.*, **57**, 2172.
13. T. J. Orzechowski, B. R. Anderson, J. C. Clark, W. M. Fawley, A. C. Paul, D. Prosnitz, E. T. Scharlemann, S. M. Yarema, A. M. Sessler, D. B. Hopkins, and J. S. Wurtele, (1986). High gain and high extraction efficiency from free electron laser amplifier operating in the millimeter wave regime. *Nucl. Instr. Meth. Phys.*, **A259**, 144.
14. A. L. Throop, T. J. Orzechowski, B. R. Anderson, F. W. Chambers, J. C. Clark, W. M. Fawley, R. A. Jong, A. C. Paul, D. Prosnitz, E. T. Scharlemann, R. D. Stever, G. A. Westenskow, and S. M. Yarema, (1987). Experimental characteristics of a high-gain free-electron laser amplifier operating at 8-mm and 2-mm wavelengths. AIM 19th Fluid Dynamics, Plasma Dynamics, and Laser Conference, Honolulu, Hawaii: June 8–10.
15. T. J. Orzechowski, E. T. Scharlemann, B. Anderson, V. K. Neil, W. M. Fawley, D. Prosnitz, S. M. Yarema, D. B. Hopkins, A. C. Paul, A. M. Sessler, and J. S. Wurtele, (1985). High-gain free electron lasers using induction linear accelerators. *IEEE J. Quantum Elec.*, **QE-21**, 831.
16. E. T. Scharlemann and W. M. Fawley, (1986). Optical modeling of induction-linac driven free-electron lasers. In *Modeling and Simulation of Optoelectronic Systems*, J. Dugan O'Keefe, ed., *Proc. SPIE*, **642**, 2–9.
17. R. A. Jong, E. T. Scharlemann, and W. M. Fawley, (1987). Wiggler taper optimization for FEL amplifiers with moderate space-charge effects. Lawrence Livermore National Laboratory, Livermore, California, UCRL-96735, presented at the Ninth International Conference on Free Electron Laser, Williamsburg, Virginia, September 14–18, 1987; to be published in *Nucl. Inst. Meth.*
18. T. J. Orzechowski, B. R. Anderson, W. M. Fawley, D. Prosnitz, E. T. Scharlemann, and S. M. Yarema, (1985). Microwave radiation from a high-gain free-electron laser amplifier. *Phys. Rev. Lett.*, **54**, 889.
19. M. Caplan, (1987). Design of a electronically tunable millimeter wave gyrotron backward wave oscillator. IEEE Twelfth International Conference on Infrared and Millimeter Waves, Orlando, Florida, December 14–18.
20. A. J. Hatch, (1966). Suppression of multipactoring in particle accelerators. *Nucl. Instr. Meth.*, **41**, 261.
21. K. Sakamoto, T. Imai, T. Fujii, Y. Ikeda, M. Saigusa, J. Sagawa, and T. Nagashima, (1986). Unipole multipactoring discharge in the LHRF launcher. *IEEE Trans. Plasma Sci.*, **PS-14**, 548.
22. E. T. Scharlemann, W. M. Fawley, B. R. Anderson, and T. J. Orzechowski, (1986). Comparison of the Livermore microwave FEL results at ELF with 2D numerical simulation. *Nucl. Instr. Meth.*, **A250**, 150.
23. R. A. Jong and E. T. Scharlemann, (1987). High gain free-electron laser for heating and current drive in the Alcator-C tokamak. *Nucl. Instr. Meth. Phys. Res.*, **A259**, 254.

24. R. A. Jong and R. R. Stone, (1988). Induction Linac-based free-electron laser amplifier for fusion applications. Lawrence Livermore National Laboratory, Livermore, California, UCRL-98675, presented at the 10th International FEL Conference, Jerusalem, Israel, August 28–September 2, 1988.
25. G. A. Deis, (1988). Lawrence Livermore National Laboratory, Livermore, California. Private communication.
26. N. M. Kroll, P. L. Morton, and M. N. Rosenbluth, (1981). Free-electron lasers with variable parameters Wigglers. *IEEE J. Quantum Elec.*, **QE-17**, 1436.
27. J. H. Van Sant, (1988). Lawrence Livermore National Laboratory, Livermore, California. Private communication.
28. G. A. Deis, (1988). Lawrence Livermore National Laboratory, Livermore, California. Private communication.
29. M. Makowski and G. Listvinsky, (1988). TRW, Redondo Beach, California. Private communication.
30. B. W. Stallard, (1988). Lawrence Livermore National Laboratory, Livermore, California. Private communication.
31. S. W. Kang, (1988). Lawrence Livermore National Laboratory, Livermore, California. Private communication.